DOE/ET/10476-T1
FE-2708-13

MASTER

Stability of SiC, Si_3N_4, Si_2N_2O, SIALON and Chromium Oxide-Containing Refractories in Coal-Gasification Environments

FINAL REPORT

DISCLAIMER

This book was prepared as an account of work sponsored by an agency of the United States Government. Neither the United States Government nor any agency thereof, nor any of their employees, makes any warranty, express or implied, or assumes any legal liability or responsibility for the accuracy, completeness, or usefulness of any information, apparatus, product, or process disclosed, or represents that its use would not infringe privately owned rights. Reference herein to any specific commercial product, process, or service by trade name, trademark, manufacturer, or otherwise, does not necessarily constitute or imply its endorsement, recommendation, or favoring by the United States Government or any agency thereof. The views and opinions of authors expressed herein do not necessarily state or reflect those of the United States Government or any agency thereof.

Arnulf Muan

College of Earth and Mineral Sciences

The Pennsylvania State University

University Park, Pennsylvania 16802

February 13, 1981

PREPARED FOR THE UNITED STATES
DEPARTMENT OF ENERGY

Under DOE/ORO Contract DE-AS05-77ET10476
(Formerly DOE Contract EF-77-S-01-2708)

APPROVED FOR RELEASE OR
PUBLICATION- O.R. PATENT GROUP
BY ELL DATE 5-1-81

DISTRIBUTION OF THIS DOCUMENT IS UNLIMITED

DISCLAIMER

This report was prepared as an account of work sponsored by an agency of the United States Government. Neither the United States Government nor any agency Thereof, nor any of their employees, makes any warranty, express or implied, or assumes any legal liability or responsibility for the accuracy, completeness, or usefulness of any information, apparatus, product, or process disclosed, or represents that its use would not infringe privately owned rights. Reference herein to any specific commercial product, process, or service by trade name, trademark, manufacturer, or otherwise does not necessarily constitute or imply its endorsement, recommendation, or favoring by the United States Government or any agency thereof. The views and opinions of authors expressed herein do not necessarily state or reflect those of the United States Government or any agency thereof.

DISCLAIMER

Portions of this document may be illegible in electronic image products. Images are produced from the best available original document.

SUMMARY

The present report summarizes the results of research performed under Contract EF-77-S-01-2708 and DE-AS05-77OR10476 during the period 9/1/77-10/31/80.

The major part of this research (the first two years of the project) was concerned with delineation of stabilities and performance characteristics of carbides and nitrides, primarily SiC, Si_3N_4 and Si_2N_2O, in slagging coal gasifiers. The data-base for evaluation of such characteristics was expanded by studying the stabilities of the above materials with respect to their oxidation by gas phases and by reaction with iron oxide-containing slag phases. This part of the research involved the following main sequential steps:

1) Application of available thermodynamic data, supplemented by additional experimental data, as needed, to evaluate stabilities of carbide-, nitride- and oxynitride phases as a function of oxygen, nitrogen and carbon activities.
2) Investigation of the nature of the reactions between liquid silicates (slags) and carbide-, nitride- and oxynitride phases.
3) Determination of the rates of reactions between liquid silicates (slags) and carbide-, nitride- and oxynitride phases.
4) Determination of temperature limits to which commercial silicon carbide refractories can be safely used in slagging coal gasifier environments.

The main conclusions of this phase of the work are as follows:

a) The refractory phases SiC, Si_3N_4 and Si_2N_2O are not stable at the oxygen potentials prevailing in slagging coal gasifiers in the temperature range 900-1500°C.
b) The corrosive action of coal-ash slags on SiC refractories is caused mainly by the reduction-oxidation reaction between SiC and the iron oxide component of the slag.

c) The rate of attack on SiC by coal-ash slag is critically dependent on temperature, i.e. whether or not the SiC-slag interface is above or below the solidus temperature of the silicates involved (as a first approximation selected compositions in the system $CaO-FeO-Al_2O_3-SiO_2$). This temperature is $\sim$ 1100°C.

Work during the third and final year of this contract was directed mainly toward delineation of equilibrium relations in chromium oxide-containing silicate systems. Main emphasis was placed on systems in which either Al_2O_3-Cr_2O_3 solid solutions or $MgAl_2O_4$-$MgCr_2O_4$ solid solutions are present as solid phases in equilibrium with slags containing the main constituents of typical coal-ash slags. Various compositions within the system $CaO-MgO-Al_2O_3-Cr_2O_3-SiO_2$ were selected initially for such studies, specifically the composition volumes $Ca_2Al_2SiO_7$-$CaAl_2Si_2O_8$-Al_2O_3-Cr_2O_3 and $Ca_2Al_2SiO_7$-$CaAl_2Si_2O_8$-$MgAl_2O_4$-$MgCr_2O_4$.

The main conclusions from these studies are as follows:

a) While the solubilities of Cr_2O_3 and chromites in the silicate melts concerned are relatively small under the atmospheric conditions usually prevailing in slagging coal gasifiers, the solubilities increase drastically at extremely low oxygen pressures, under which conditions a substantial fraction of the chromium is present in the silicate liquid as Cr^{2+}. The oxygen pressures at which this situation prevails, however, are somewhat lower than those usually prevailing in coal gasification atmospheres.

b) The lowest liquidus and solidus temperatures in the systems $Ca_2Al_2SiO_7$-$CaAl_2Si_2O_8$-$MgCr_2O_4$ systems are not significantly below those of the $Ca_2Al_2SiO_7$-$CaAl_2Si_2O_8$ join ($\sim$ 1387°C) because of the relatively low solubility of Cr_2O_3 (and $MgCr_2O_4$) in these silicate melts, as noted above. With increasing Al_2O_3/Cr_2O_3 ratios of the refractory phases, however, the lowest

liquidus and solidus temperatures decrease considerably, as larger amounts of Al_2O_3 or $MgAl_2O_4$ of the refractory phase dissolve in the silicate liquid.

c) The mutual solubilities between Al_2O_3- and Cr_2O_3 end members in the system $CaO-Al_2O_3-Cr_2O_3$ are rather limited. Two new ternary compounds, "E" and "L", have been synthesized, with compositions approximately as follows:

"E": 19 wt.% CaO, 38 wt.% Al_2O_3, 43 wt.% Cr_2O_3

"L": 44 wt.% CaO, 33 wt.% Al_2O_3, 23 wt.% Cr_2O_3 .

d) A quinary compound has been found in the system $CaO-MgO-Al_2O_3-Cr_2O_3-SiO_2$, with composition approximately as follows: 15 wt.% CaO, 6 wt.% MgO, 40 wt.% Al_2O_3, 30 wt.% Cr_2O_3, 9 wt.% SiO_2.

The overall time schedule for work on the various tasks is shown in Fig. 1.

RESULTS

Stabilities of SiC, Si_3N_4 and Si_2N_2O

The diagrams presented in Figs. 2-3 summarize in simple graphical form interrelations between oxygen potentials of typical coal gasification atmospheres and stability ranges of the various carbide-, nitride- and oxynitride phases as a function of temperature. The first diagram (Fig. 2) illustrates relations for SiC. The solid curve in the lower part of the diagram represents the equilibrium between SiO_2 (stable in the area above the curve) and SiC (stable in the area below the curve) at a CO pressure of 1 atm. The dash curves above and below the solid curve depict the same equilibrium (i.e. coexistence of SiO_2 and SiC) at CO-pressures of 50 and 0.02 atm., respectively. It is seen that over the entire temperature range covered ($\sim$ 800-1600°C), and at the three CO pressures used as examples, the SiO_2/SiC equilibrium curves are located far below the shaded area representing approximate oxygen potentials

(in terms of the function R'T $\log_{10} P_{O_2}$ as plotted along the vertical axis) of typical coal gasification atmospheres.

Similar relations apply in the case of silicon nitride and oxynitride, as demonstrated in Fig. 3. The solid curves in the lower part of the diagram show the equilibrium curves for SiO_2/Si_2N_2O and $Si_2N_2O/\alpha\text{-}Si_3N_4$ at an N_2 pressure of 10^{-2} atm. The dash and dash-dot curves represent the SiO_2/Si_2N_2O equilibrium at N_2 pressures of 1 atm. and 10^{-4} atm., respectively. It is seen that the SiO_2/Si_2N_2O curves, at all three N_2 pressures considered, are located far below the shaded area representing approximate oxygen potentials of typical coal gasification atmospheres. Hence, the typical coal gasification atmospheres are strongly oxidizing relative to these nitride- and oxynitride phases.

Nature of Reactions between SiC or Si_3N_4 and Various Oxide Constituents, Including Slags

Reactions between simplified slags and SiC or Si_3N_4 have shown that only small to moderate depressions of the known liquidus temperatures of the oxide phases takes place when the latter are made up from oxide components of very high thermodynamic stability, i.e. of large negative standard free energies of formation (e.g. CaO, Al_2O_3, SiO_2 etc.). This is an indication that relatively small amounts of C and N are dissolved in the largely oxidic liquids present. At elevated pressures (e.g. 68 atm.), these effects are undoubtedly somewhat larger than at 1 atm., but they are still expected to be relatively minor. There is one component of coal-ash slags, however, which behaves quite differently, viz. iron oxide (FeO and/or Fe_2O_3). This oxide is much less stable relative to its constituent elements than are the oxides previously mentioned (CaO, MgO, Al_2O_3, SiO_2), as illustrated by the standard-free energy curves (ΔG°) shown in Fig. 4. Hence, in the case of FeO, this component of the slag

will have a tendency to react with SiC according to the simplified equation

$$SiC + 3(FeO) = SiO_2 + 3[Fe] + CO \qquad (1)$$

The change in standard free energy of this reaction is relatively small ($\sim$ -20 Kcal). Hence equilibrium between SiC, the oxidation product SiO_2, metallic iron and FeO of the slag is reached at a moderately low FeO-concentration of the slag. Metallic iron will tend to be precipitated from the slag at or near the SiC refractory-slag interface until the FeO activity has been lowered to the equilibrium value required by equation (1).

That this reaction actually takes place at the SiC-slag interface has been shown in testing of SiC brick corrosion by actual coal-ash slags and by laboratory reactions between SiC and FeO-containing silicate melts, as illustrated by sketches shown in Fig. 5.

The reaction between SiC and FeO of the slag, as described above, serves to remove part of the FeO component from the slag. The equilibrium relations in the remaining oxide system may then, as a first approximation, be discussed in terms of the system $CaO-Al_2O_3-SiO_2$. This is shown in Fig. 6, illustrating the liquidus surface of this system and showing as a black circle the approximate composition of FeO-depleted coal-ash slags in terms of the components used in this diagram. The solidus surface of the same system ($CaO-Al_2O_3-SiO_2$) is sketched in Fig. 7, with the black circle again representing approximate compositions of FeO-depleted coal-ash slags. It is seen that the solidus temperatures for a mixture of this composition, and consisting mainly of anorthite, with lesser amounts of silica and wollastonite, is $\sim$ 1100°C. It is inferred that the SiC-slag interface must be cooled to temperatures below this level in order to provide a reasonable measure of protection for a SiC refractory against oxidation-corrosion by coal-ash slags (see section on kinetics below).

Inasmuch as the reaction between SiC and the FeO of the slag removes only a part of the FeO component of the slag, a more accurate picture of equilibrium relations attending the reaction is afforded by consideration of phase relations in parts of the system CaO-"FeO"-Al_2O_3-SiO_2, as illustrated in Figs. 8-10. The first of these (Fig. 8) is a perspective drawing of a tetrahedron representing this system and showing the various composition volumes. The parts of the tetrahedron of greatest interest in the present research are the volumes and the bounding triangles in the vicinity of the SiO_2 apex, i.e. $CaAl_2Si_2O_8$-$CaSiO_3$-FeO-SiO_2. Phase relations in two of the ternary systems bounding this quaternary system are portrayed in Figs. 9 and 10. The solidus temperatures are of the order of $\sim$ 1080-1120°C, thus establishing an upper limit for the temperature that may be tolerated without severe fluxing-oxidation of a SiC refractory by coal-ash slags, in accordance with considerations presented in the following section. The actual practical temperature limit may be considerably lower, however.

Kinetics of Reactions between SiC and Oxidizing Atmospheres, with or without Oxide (Slag) Phases Present

A large volume of literature is available on the oxidation of SiC. These previous studies have established that the reaction is usually characterized by the formation of a dense SiO_2 layer on the surface of the SiC, and that the rate of oxidation is dependent primarily on the rate of diffusion of oxygen through this layer. Inasmuch as this diffusion rate is low under most circumstances, the rate of oxidation at moderate temperatures is usually quite low. However, continued protection against oxidation of the remaining SiC is dependent on the preservation of the SiO_2 protective layer. Hence, a slag having constituents reacting with SiO_2 to remove this layer would have a strong

detrimental effect on the ability of the SiC body to withstand corrosion by oxidation. It is clear that the rate and mechanism by which the protective SiO_2 layer is removed by reaction with the slag is a critical factor in evaluating behavior of SiC refractories in a coal gasification environment.

Representative results of the rates of the SiC-gas reactions, as determined in the present research, are shown in Figs. 11-14. The first of these (Fig. 11) shows results of oxidation of SiC in O_2-argon atmospheres at 1100, 1200 and 1300°C. The most striking feature of the graph is the progressive decrease in the dependence of the parabolic rate constant K with increasing temperature ($[1-(1-F)^{1/3}]^2 = Kt$, where F is fraction of SiC reacted and t is the time).

The next diagram (Fig. 12) shows some typical results of experiments involving the oxidation of SiC pellets in various CO_2-containing atmospheres. The calculated activation energies for the oxidation under these conditions was found to be relatively constant ($\sim$ 75 Kcal) in the temperature range of 1100-1300°C.

The effects of the presence of admixtures of some silicate phases on the oxidation of SiC in a CO_2/CO atmosphere are illustrated in Fig. 13. Included for comparison is a curve for SiC without the addition of an oxide phase.

Data obtained for the kinetics of the reaction between FeO and SiC in CO_2-CO atmospheres are shown in Fig. 14. An activation energy of $\sim$ 50 Kcal is calculated from these data.

Effects of Strongly Reducing Conditions on Equilibria in Chromium Oxide-Containing Systems

Liquidus and solidus temperatures in systems containing chromium oxide as a component may decrease drastically at very low oxygen potentials, where

substantial proportions of the chromium is present as Cr^{2+} in the silicate melts. This is illustrated for the systems chromium oxide-SiO_2 and Al_2O_3-chromium oxide-SiO_2 in contact with metallic chromium, in Figs. 15 and 16, respectively.

Experimental studies of these systems have also been carried out at somewhat higher oxygen potentials. This is based on the observation that the presence of Cr^{2+} in amounts large enough to change significantly the phase relations observed in Cr_2O_3-containing systems is restricted to a range of very low oxygen pressures. It was considered essential that the extent of this range be established for at least a couple of systems. Toward this end, the solidus temperatures as a function of oxygen pressure were determined experimentally for the systems chromium oxide-SiO_2 and chromium oxide-Al_2O_3-SiO_2. The results are summarized in Fig. 17. It is clear that the oxygen partial pressures of the gas phase in slagging coal gasifiers usually is higher than those at which the presence of Cr^{2+} in the slag phase has a noticeably depressing effect on solidus (and liquidus) temperatures of the refractory. However, Cr^{2+} may play a role in the chemistry of coal-ash slags at the SiC-slag interface, especially at the highest temperatures ($\sim$ 1600°C) involved.

Equilibrium Relations in the System CaO-Al_2O_3-Cr_2O_3 in CO_2-H_2 Atmosphere

Phase relations in the system CaO-Al_2O_3-Cr_2O_3 have been determined in the solidus temperature region CO_2-H_2 atmospheres of mixing ratio 10:1. The results obtained are summarized graphically in Fig. 18. Most noteworthy among the relations shown is the occurrence of two previously unreported ternary phases. One of these (designated "L" in the diagram) has a composition of approximately 44 wt.% CaO, 33 wt.% Al_2O_3 and 23 wt.% Cr_2O_3. The other phase (designated "E" in the diagrams) has a composition of approximately 19 wt.% CaO, 38 wt.% Al_2O_3 and 43 wt.% Cr_2O_3.

In the bounding binary system $CaO-Cr_2O_3$, there is only one stable compound, $CaCr_2O_4$, whereas in the system $CaO-Al_2O_3$ a large number of calcium aluminates are stable, viz. $Ca_3Al_2O_6$, $Ca_{12}Al_{14}O_{33}$, $CaAl_2O_4$, $CaAl_4O_7$, $CaAl_{12}O_{19}$. There is a complete solid-solution series between Al_2O_3 and Cr_2O_3 to form the sesquioxide phase in which at high temperatures (> ∿ 1100°C) Cr^{3+} and Al^{3+} substitute for each other in all proportions. The degree of substitution of Cr^{3+} for Al^{3+} in the various calcium aluminates varies greatly with $CaO/(Al_2O_3+Cr_2O_3)$ ratios of the phase, decreasing, in general, with increasing values of this ratio. A substantial amount (∿ 20%) of Al^{3+} substitutes for Cr^{3+} in $CaCr_2O_4$ at the high temperatures involved in the present study. The lowest solidus temperatures in the system are for mixtures of relatively high CaO- and Al_2O_3 contents (composition triangles $CaO-CaCr_2O_4$-"L", CaO-"L"-$Ca_3Al_2O_6$, "L"-$Ca_3Al_2O_6$-$Ca_{12}Al_{14}O_{33}$, and "L"-$Ca_{12}Al_{14}O_{33}$-$CaAl_2O_4$).

Equilibrium Relations in the System $FeO-Al_2O_3-Cr_2O_3-SiO_2$

The equilibrium studies in this system were carried out over a range of controlled oxygen partial pressures similar to those involved in slagging coal gasifiers. The results obtained demonstrate that there is a profound effect of oxygen pressure on the distribution of chromium between solid phases (i.e. refractory phases) and silicate liquids (i.e. slags) at very low oxygen pressures. For instance, the solubility of chromium oxide in the silicate liquid in equilibrium with the crystalline phases SiO_2, mullite, sesquioxide (Al_2O_3-Cr_2O_3 solid solution), spinel ($FeAl_2O_4$-$FeCr_2O_4$-$FeFe_2O_4$ solid solution) increases by a factor of ∿ 8 as the oxygen pressure decreases from ∿ 10^{-9} to ∿ 10^{-12} atm. at ∿ 1400°C. This is illustrated in Fig. 19. No drastic effect of changing oxygen pressures on the solidus and liquidus temperatures for this phase assemblage in the system Fe-Cr-Al-Si-O is observed. This is because the

iron-oxide content of the liquid phase decreases concomitantly with the increase in chromium oxide content (Cr^{2+}) as the oxygen pressure decreases from $\sim 10^{-9}$ to $\sim 10^{-12}$ atm. at $\sim$ 1400°C.

Equilibrium Relations in the System $Ca_2Al_2SiO_7$-$CaAl_2Si_2O_8$-Al_2O_3-Cr_2O_3 in CO_2-H_2 Atmosphere

The system CaO-Al_2O_3-Cr_2O_3-SiO_2 is portrayed in the form of a regular tetrahedron in Fig. 20. The compositions of the two ternary compounds gehlenite ($Ca_2Al_2SiO_7$) and anorthite ($CaAl_2Si_2O_8$) are shown in the basal plane. Combination of these two points with the two apices Al_2O_3 and Cr_2O_3 describes an irregular tetrahedron representing the sub-system $Ca_2Al_2SiO_7$-$CaAl_2Si_2O_8$-Al_2O_3-Cr_2O_3. Phase relations in one of the bounding planes of this tetrahedron, viz. $Ca_2Al_2SiO_7$-$CaAl_2Si_2O_8$-Al_2O_3, are known from previous work, as shown in Fig. 21.

Phase relations in the bounding plane $Ca_2Al_2SiO_7$-$CaAl_2Si_2O_8$-Cr_2O_3 were determined in the present work. Results obtained are shown graphically in Fig. 22. Attention is directed toward the very low solubility of chromium oxide ($\sim$ 0.5 wt.% Cr_2O_3) in the silicate liquid and the relatively low depression of liquidus temperatures (temperature of the ternary eutectic point $\sim$ 1380°C as compared with an eutectic temperature of 1387°C in the binary system $Ca_2Al_2SiO_7$-$CaAl_2Si_2O_8$). Attention is also directed toward the much higher solubility of Al_2O_3 in the corresponding silicate liquids in the system $Ca_2Al_2SiO_7$-$CaAl_2Si_2O_8$-Al_2O_3 (see Fig. 21).

Equilibrium Relations in the System $Ca_2Al_2SiO_7$-$CaAl_2Si_2O_8$-$MgAl_2O_4$-$MgCr_2O_4$ in CO_2-H_2 Atmosphere

The system $Ca_2Al_2SiO_7$-$CaAl_2Si_2O_8$-$MgAl_2O_4$-$MgCr_2O_4$ is portrayed in the form of a regular tetrahedron in Fig. 23. The join $Ca_2Al_2SiO_7$ (gehlenite)-$CaAl_2Si_2O_8$

(anorthite) represents simplified compositions of typical coal-ash slags, and the remaining two apices of the tetrahedron ($MgAl_2O_4$ and $MgCr_2O_4$) represent end-member refractory spinels. Phase relations existing in two of the faces of this tetrahedron, viz. $Ca_2Al_2SiO_7$-$CaAl_2Si_2O_8$-$MgAl_2O_4$ and $Ca_2Al_2SiO_7$-$CaAl_2Si_2O_8$-$MgCr_2O_4$, are shown in Figs. 24-25. The first of these (Fig. 24) shows approximate phase relations in the system $Ca_2Al_2SiO_7$-$CaAl_2Si_2O_8$-$MgCr_2O_4$ in an atmosphere of CO_2-H_2 = 10:1. The second diagram (Fig. 25) shows approximate liquidus phase relations in the system $Ca_2Al_2SiO_7$-$CaAl_2Si_2O_8$-$MgAl_2O_4$ in CO_2-H_2 atmosphere of CO_2/H_2 ratio = 10:1.

The crystalline phase designated "Y" in Fig. 24 has been found, by electron microprobe analysis, to have approximately the following compositions: 15 wt.% CaO, 6 wt.% MgO, 40 wt.% Al_2O_3, 30 wt.% Cr_2O_3, 9 wt.% SiO_2.

LEGENDS FOR DIAGRAMS

Fig. 1 Summary of time schedules for various aspects of the research. The width of the bars is a measure of the relative efforts of the various tasks performed.

Fig. 2 Curves (see lower part of diagram) showing the SiO_2/SiC equilibrium at CO-pressures of 1 atm. (solid line), 50 and 0.02 atm. (dash lines) as a function of temperature. The shaded area in the upper part of the diagram indicates approximate oxygen potentials of typical coal gasification atmospheres.

Fig. 3 Curves (see lower part of diagram) showing the SiO_2/Si_2N_2O and $Si_2N_2O/\alpha\text{-}Si_3N_4$ equilibria at N_2 pressures of 10^{-2} atm. (solid line), 1 atm. (dash line) and 10^{-4} atm. (dash-dot line). The shaded area in the upper part of the diagram indicates approximate oxygen potentials of typical coal gasification atmosphere.

Fig. 4 Standard free energies ($\Delta G°$) of formation of various oxides from their elements[1].

Fig. 5 Sketches showing typical features of reactions between SiC and FeO-containing coal-ash slags, as observed in testing of refractories (a) and in laboratory-scale experiments (b).

Fig. 6 Liquidus surface of the system $CaO\text{-}Al_2O_3\text{-}SiO_2$, reproduced from Muan and Osborn[1], based on data available in previous literature[2-7].

Fig. 7 Solidus surface of the system $CaO\text{-}Al_2O_3\text{-}SiO_2$, sketched on the basis of data shown in Fig. 6.

Fig. 8 Sketch of tetrahedron representing the system $CaO\text{-}FeO\text{-}Al_2O_3\text{-}SiO_2$, showing the composition volumes of main interest in conjunction with coal-ash slags.

Fig. 9. Liquidus phase relations in part of the system CaO-FeO-Al_2O_3-SiO_2, based on data of Schairer[8].

Fig. 10 Liquidus phase relations in part of the system CaO-FeO-Al_2O_3-SiO_2, based on data of Schairer[8].

Fig. 11 Parabolic rate constants as a function of oxygen pressure at various temperatures (1100, 1200, 1300°C) for oxidation of SiC pellets in O_2-Ar mixtures.

Fig. 12 Parabolic rate constants as a function of CO_2 pressure at various temperatures (1200, 1250, 1300°C) for oxidation of SiC pellets in various CO_2-containing atmospheres.

Fig. 13 Rates of oxidation of SiC pellets with and without additions of various oxide phases, as labelled on each curve, at a constant temperature of 1100°C.

Fig. 14 Rates of oxidation of SiC pellets with additions of various amounts of FeO, as labelled on each curve, at a constant temperature of 1000°C.

Fig. 15 Phase relations in the system chromium oxide-SiO_2 in contact with metallic chromium.

Fig. 16 Liquidus phase relations in the system Al_2O_3-chromium oxide-SiO_2 in contact with metallic chromium.

Fig. 17 Effects of oxygen pressure on solidus temperatures in SiO_2-chromium oxide and Al_2O_3-chromium oxide-SiO_2 mixtures.

Fig. 18 Approximate solidus surface of the system CaO-Al_2O_3-Cr_2O_3 in a CO_2-H_2 atmosphere of ratio 10:1. The composition of two ternary compounds designated as "L" and "E" are approximately as shown, although further analytical work is needed to characterize these phases more accurately.

Fig. 19 Variation in chromium oxide content of liquid of phase assemblage SiO_2 + mullite + spinel + sesquioxide + liquid in the system Fe-Cr-Al-Si-O at ∿ 1400°C, as a function of oxygen pressure.

Fig. 20 Perspective drawing of tetrahedron representing the system CaO-Al_2O_3-Cr_2O_3-SiO_2. The composition volume of especial interest in the present work is $Ca_2Al_2SiO_7$-$CaAl_2Si_2O_8$-Al_2O_3-Cr_2O_3.

Fig. 21 Sketch showing main features of liquidus phase relations in the system $Ca_2Al_2SiO_7$-$CaAl_2Si_2O_8$-Al_2O_3, reproduced from Muan and Osborn[1], based largely on the original data of Rankin and Wright[2] and of Greig[3], with modifications based on more recent data[4-7].

Fig. 22 Sketch showing main features of liquidus phase relations in the system $Ca_2Al_2SiO_7$-$CaAl_2Si_2O_8$-Cr_2O_3 in a CO_2-H_2 atmosphere of ratio 10:1, as determined in the present investigation.

Fig. 23 Tetrahedron representing the system $Ca_2Al_2SiO_7$-$CaAl_2Si_2O_8$-$MgAl_2O_4$-$MgCr_2O_4$, showing representative planes of constant $MgAl_2O_4/MgCr_2O_4$ ratios of mixtures.

Fig. 24 Approximate liquidus phase relations in the system $Ca_2Al_2SiO_7$-$CaAl_2Si_2O_8$-$MgCr_2O_4$ in an atmosphere of CO_2-H_2 = 10:1. Heavy lines are boundary curves outlining the various primary phase fields, and light lines are liquidus isotherms.

Fig. 25 Approximate liquidus phase relations in the system $Ca_2Al_2SiO_7$-$CaAl_2Si_2O_8$-$MgAl_2O_4$, as reproduced from previous literature[9]. Heavy lines are boundary curves outlining the various primary phase fields, and light lines are liquidus isotherms.

REFERENCES

1. A. Muan and E. F. Osborn. Phase Equilibria among Oxides in Steelmaking. Addison-Wesley Publishing Co., Reading, Massachusetts. (1965) 236 pp.
2. G. A. Rankin and F. E. Wright. The Ternary System $CaO-Al_2O_3-SiO_2$. Am. J. Sci. (4th Series), 1915, v. 39, pp. 1-79.
3. J. W. Greig. Immiscibility in Silicate Melts. Am. J. Sci. (5th Series), 1927, v. 13, pp. 1-44, 133-154.
4. N. E. Filonenko and I. V. Lavrov. Investigations of Equilibrium Conditions in the Al_2O_3 Corner of the System $CaO-Al_2O_3-SiO_2$. Zhur. Priklad. Khim. (U.S.S.R.), 1950, v. 23, pp. 1040-1046; J. Appl. Chem. (U.S.S.R.), 1950, v. 23, pp. 1105-1112 (English Translation); Chem. Abstr., 1952, v. 46, p. 786a.
5. F. C. Langenberg and J. Chipman, Determination of 1600°C and 1700°C Liquidus Lines in $CaO \cdot 2A_2O_3$ and Al_2O_3 Stability Fields of the System $CaO-Al_2O_3-SiO_2$. J. Am. Ceram. Soc., 1965, v. 39, pp. 423-433.
6. S. Aramaki and R. Roy. The Mullite-Corundum Boundary in the Systems $MgO-Al_2O_3-SiO_2$ and $CaO-Al_2O_3-SiO_2$. J. Am. Ceram. Soc., 1959, v. 42, pp. 644-645.
7. A. L. Gentile and W. R. Foster. Calcium Hexaluminate and Its Stability Relations in the System $CaO-Al_2O_3-SiO_2$. J. Am. Ceram. Soc., 1963, v. 46, pp. 74-76.
8. J. F. Schairer, The System $CaO-FeO-Al_2O_3-SiO_2$. I. Results of Quenching Experiments on Five Joins. J. Am. Ceram. Soc., 25, 241-274 (1942).
9. G. W. Morey. Phase-Equilibrium Relations of the Common Rock-Forming Oxides except Water. Chapter L of Data on Geochemistry, M. Fleischer, Technical Editor, U.S. Government Printing Office, Washington, D.C., 1964.

PROJECTED TIME SCHEDULE FOR VARIOUS TASKS

DOE PROJECT NO. EF-77-S-01-2708

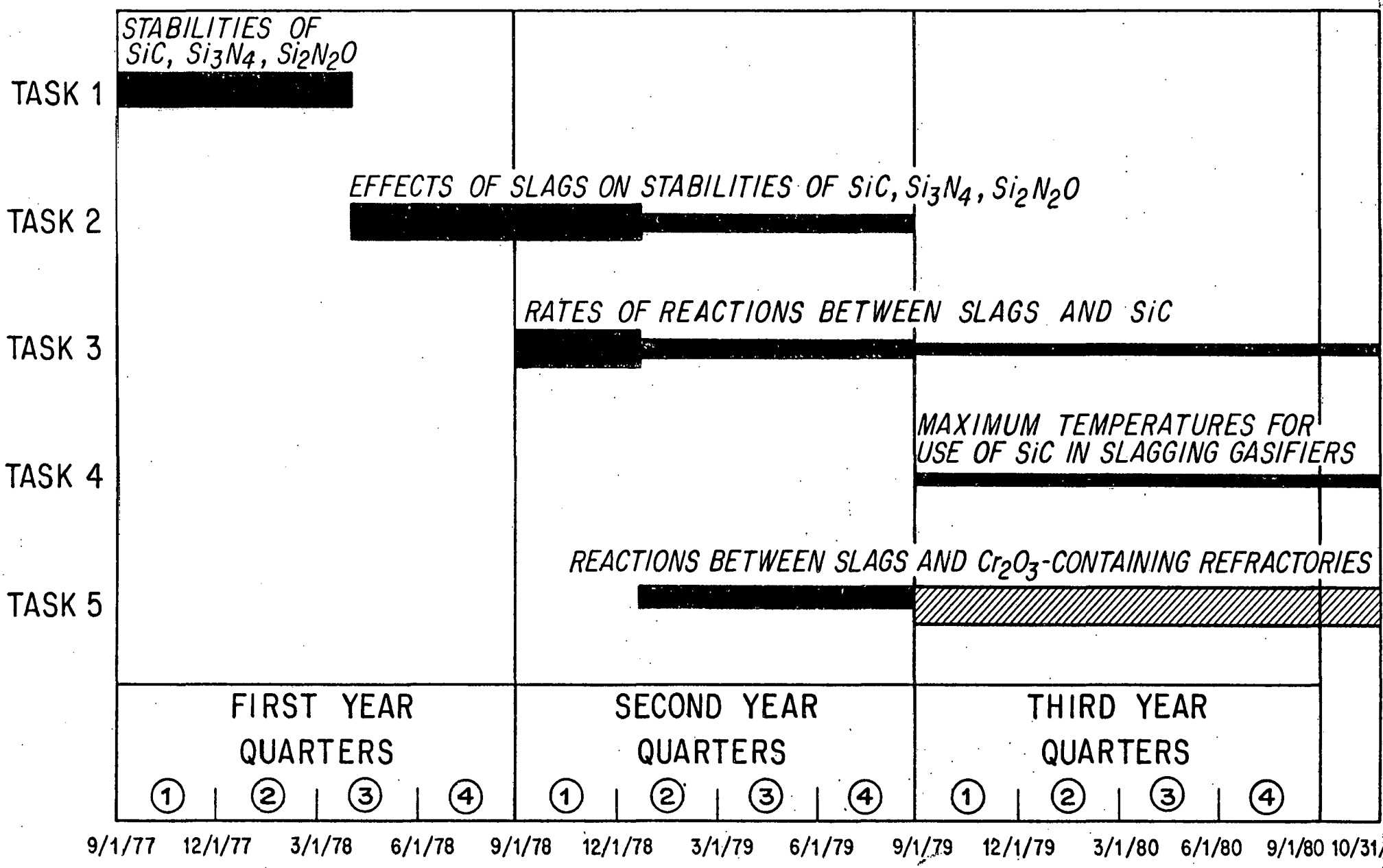

Fig. 1

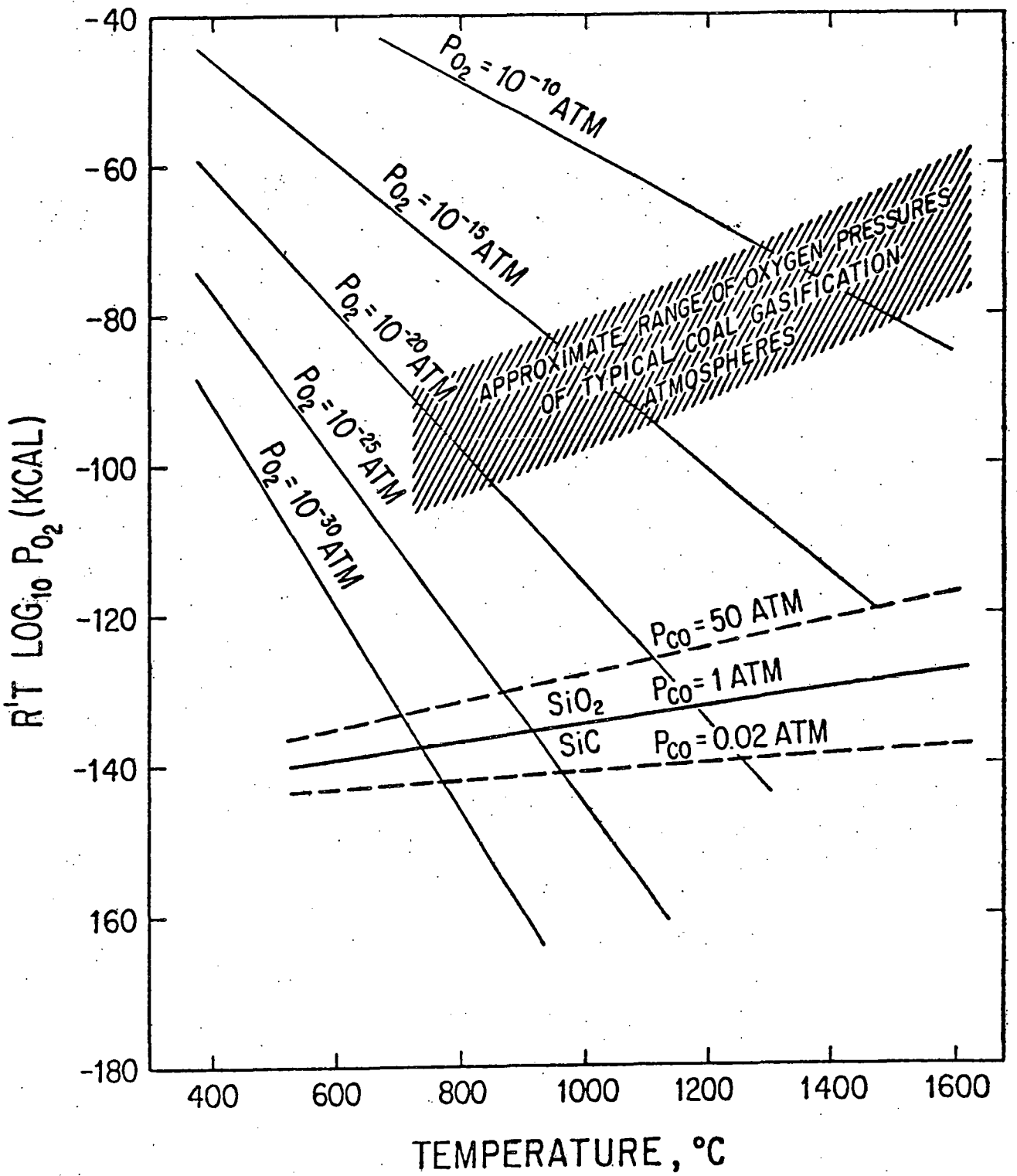
-40
-60
-80
-100
-120
-140
160
-180
400
600
800
1000
1200
1400
1600
TEMPERATURE, °C
R'T LOG10 PO2 (KCAL)
PO2 = 10-10 ATM
PO2 = 10-15 ATM
PO2 = 10-20 ATM
PO2 = 10-25 ATM
PO2 = 10-30 ATM
APPROXIMATE RANGE OF OXYGEN PRESSURES OF TYPICAL COAL GASIFICATION ATMOSPHERES
PCO = 50 ATM
PCO = 1 ATM
PCO = 0.02 ATM
SiO2
SiC

Fig. 2

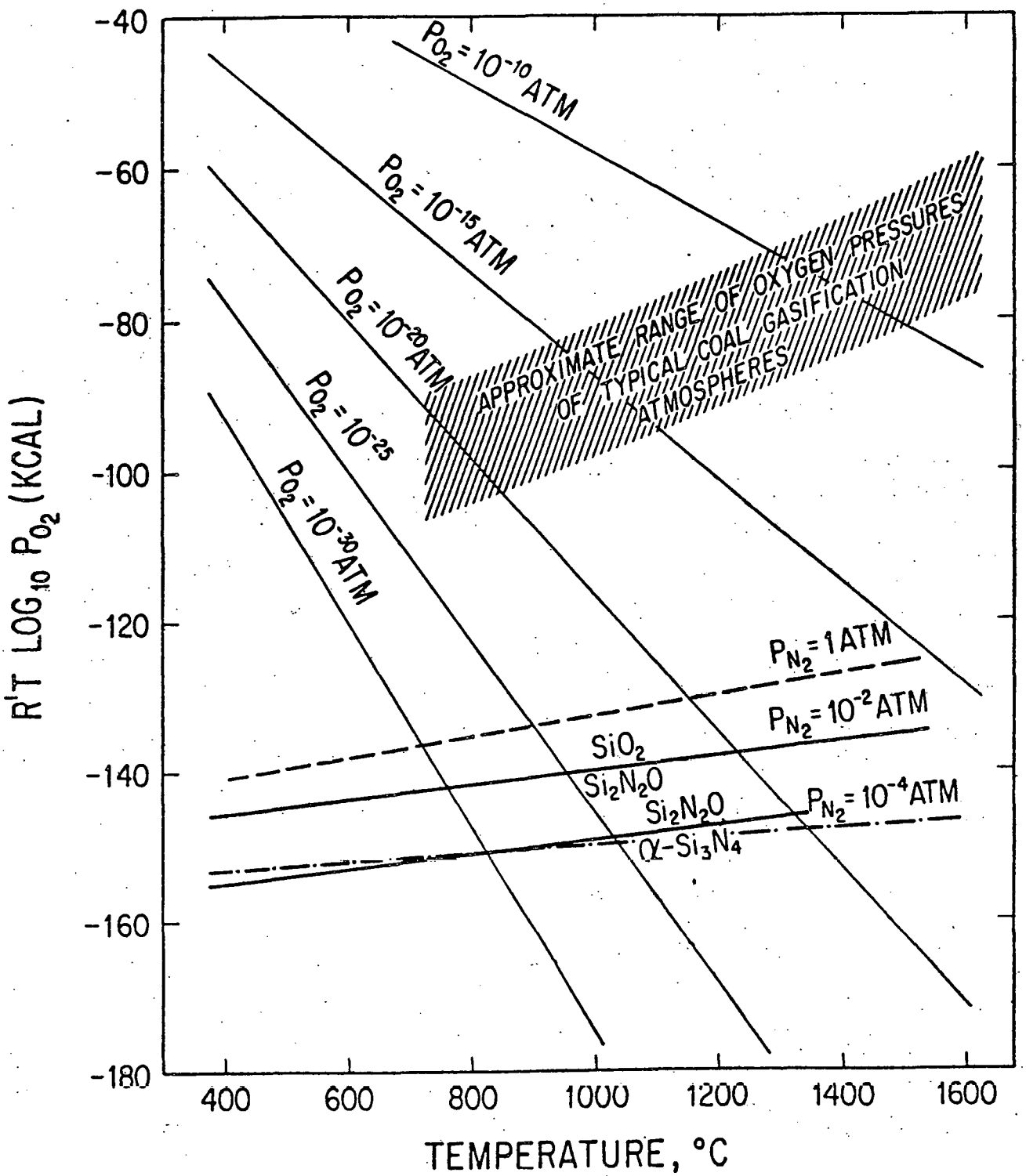
-40
-60
-80
-100
-120
-140
-160
-180
400
600
800
1000
1200
1400
1600
R'T LOG10 PO2 (KCAL)
TEMPERATURE, °C
PO2 = 10-10 ATM
PO2 = 10-15 ATM
PO2 = 10-20 ATM
PO2 = 10-25
PO2 = 10-30 ATM
APPROXIMATE RANGE OF OXYGEN PRESSURES OF TYPICAL COAL GASIFICATION ATMOSPHERES
PN2 = 1 ATM
PN2 = 10-2 ATM
PN2 = 10-4 ATM
SiO2
Si2N2O
Si2N2O
α-Si3N4

Fig. 3

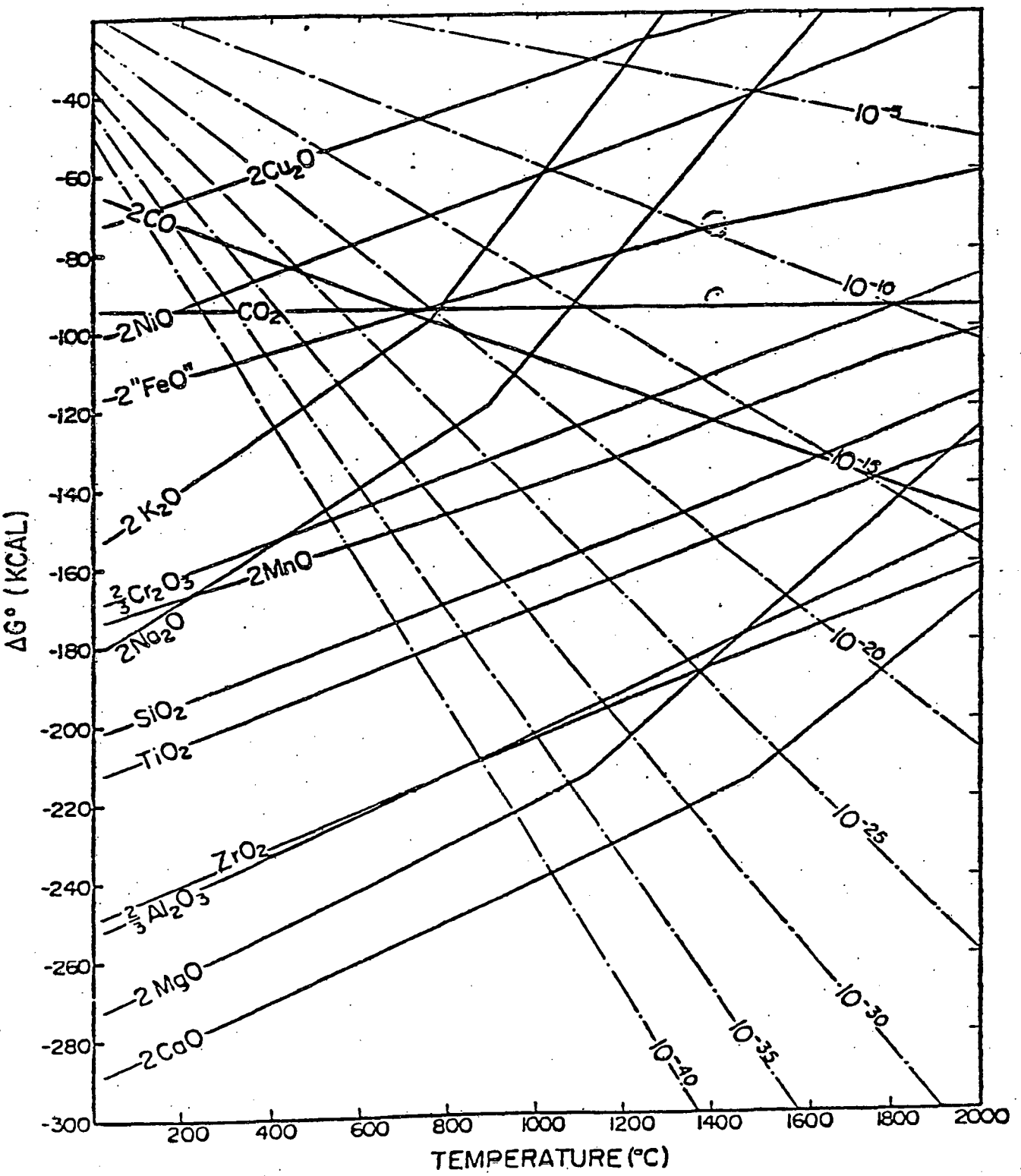
ΔG° (KCAL)
TEMPERATURE (°C)
-40
-60
-80
-100
-120
-140
-160
-180
-200
-220
-240
-260
-280
-300
200
400
600
800
1000
1200
1400
1600
1800
2000
2Cu2O
2CO
2NiO
CO2
2"FeO"
2K2O
2/3Cr2O3
2MnO
2Na2O
SiO2
TiO2
ZrO2
2/3Al2O3
2MgO
2CaO
C
C
10-5
10-10
10-15
10-20
10-25
10-30
10-35
10-40

Fig. 4

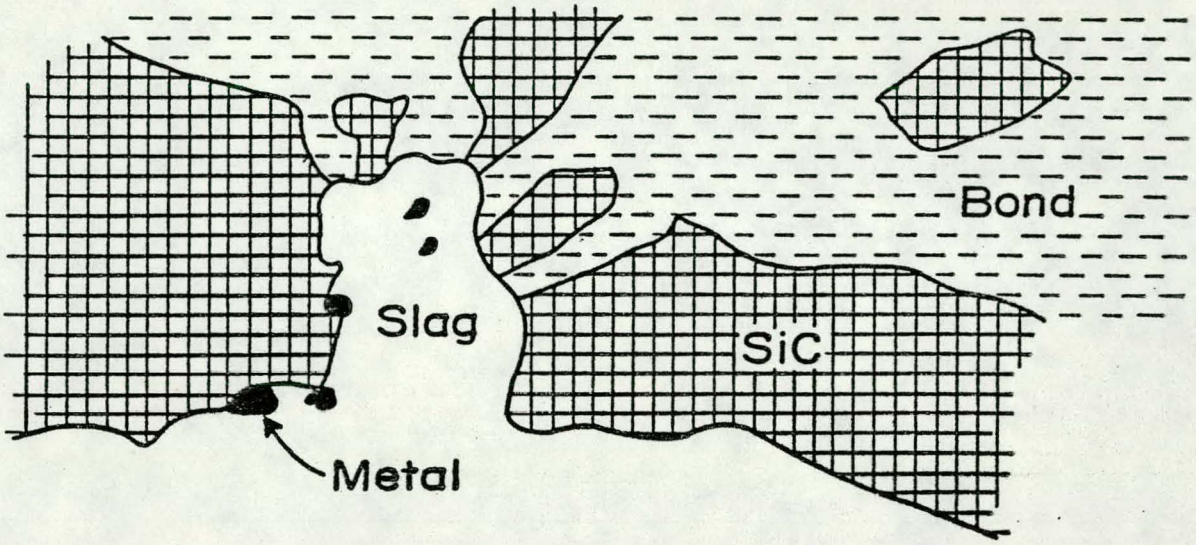
Bond
Slag
SiC
Metal

(a)

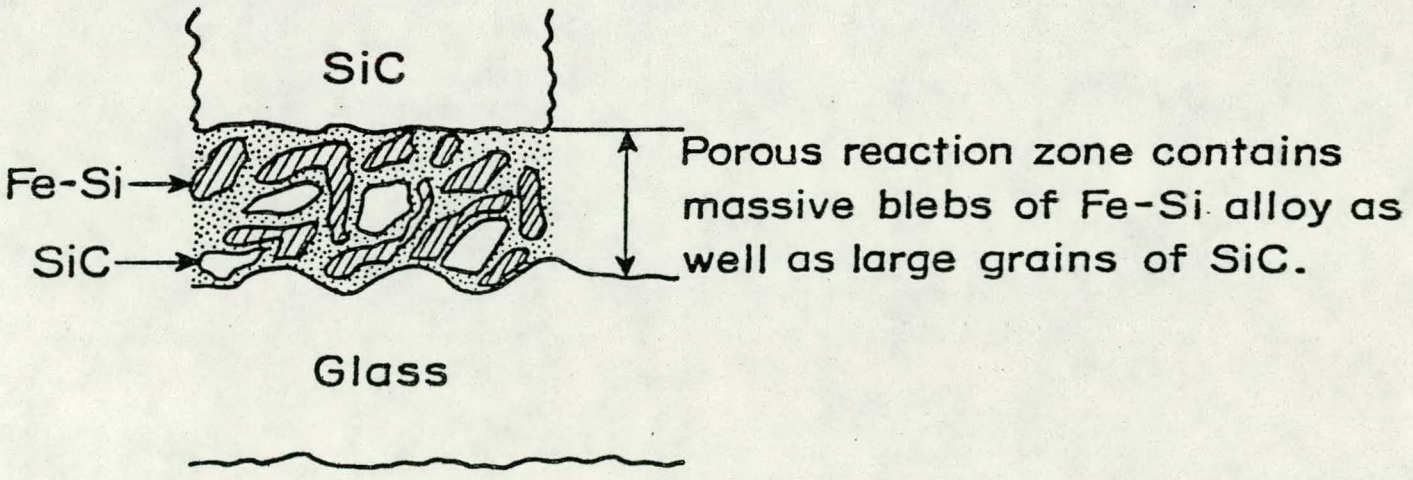
SiC
Fe-Si
SiC
Porous reaction zone contains massive blebs of Fe-Si alloy as well as large grains of SiC.
Glass

(b)

Fig. 5

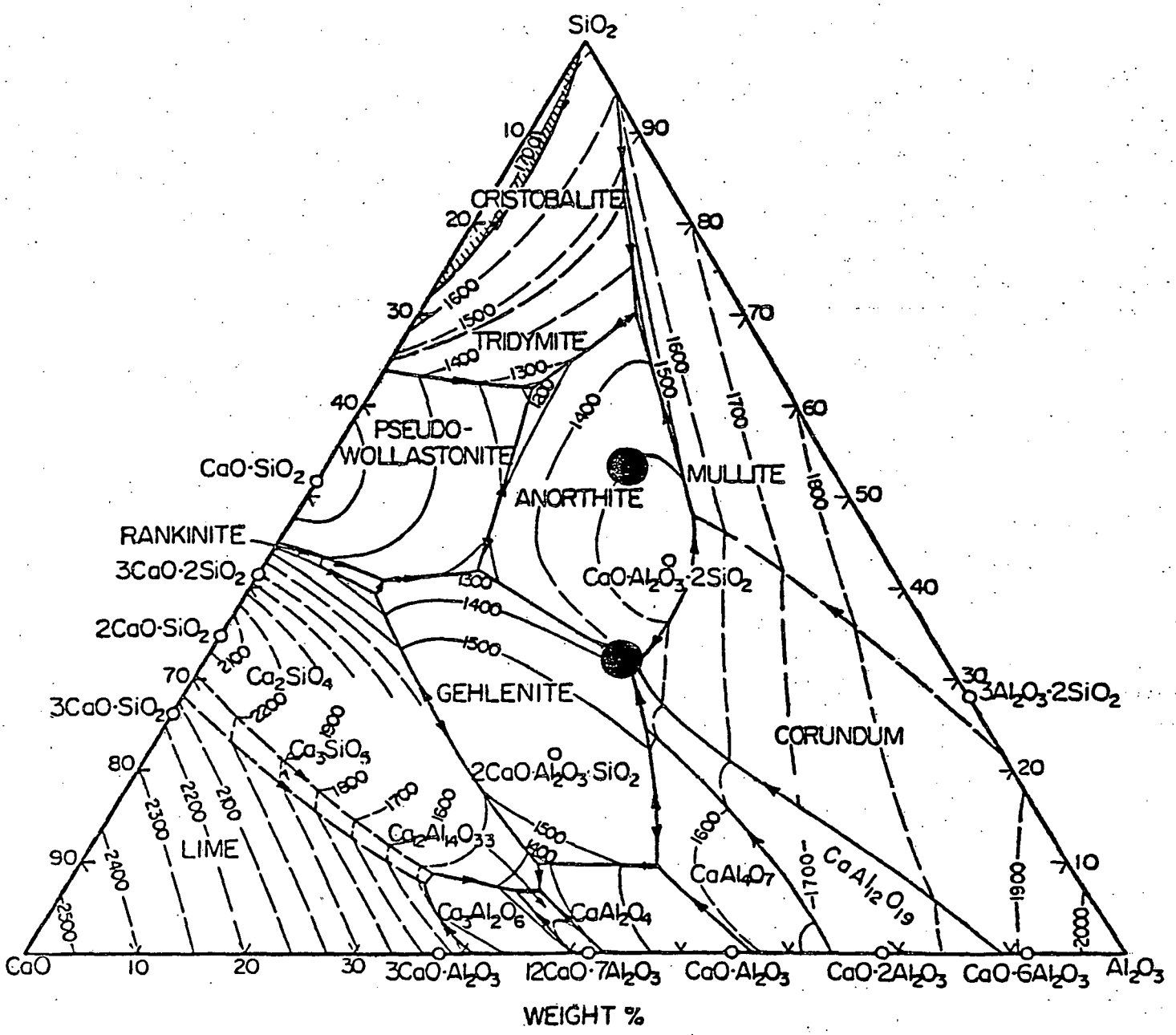
SiO2
CRISTOBALITE
TRIDYMITE
PSEUDO-
WOLLASTONITE
CaO·SiO2
RANKINITE
3CaO·2SiO2
2CaO·SiO2
Ca2SiO4
3CaO·SiO2
Ca3SiO5
LIME
ANORTHITE
MULLITE
CaO·Al2O3·2SiO2
GEHLENITE
2CaO·Al2O3·SiO2
Ca2Al14O33
Ca3Al2O6
CaAl2O4
CaAl4O7
CaAl12O19
CORUNDUM
3Al2O3·2SiO2
CaO
3CaO·Al2O3
12CaO·7Al2O3
CaO·Al2O3
CaO·2Al2O3
CaO·6Al2O3
Al2O3
WEIGHT %

Fig. 6

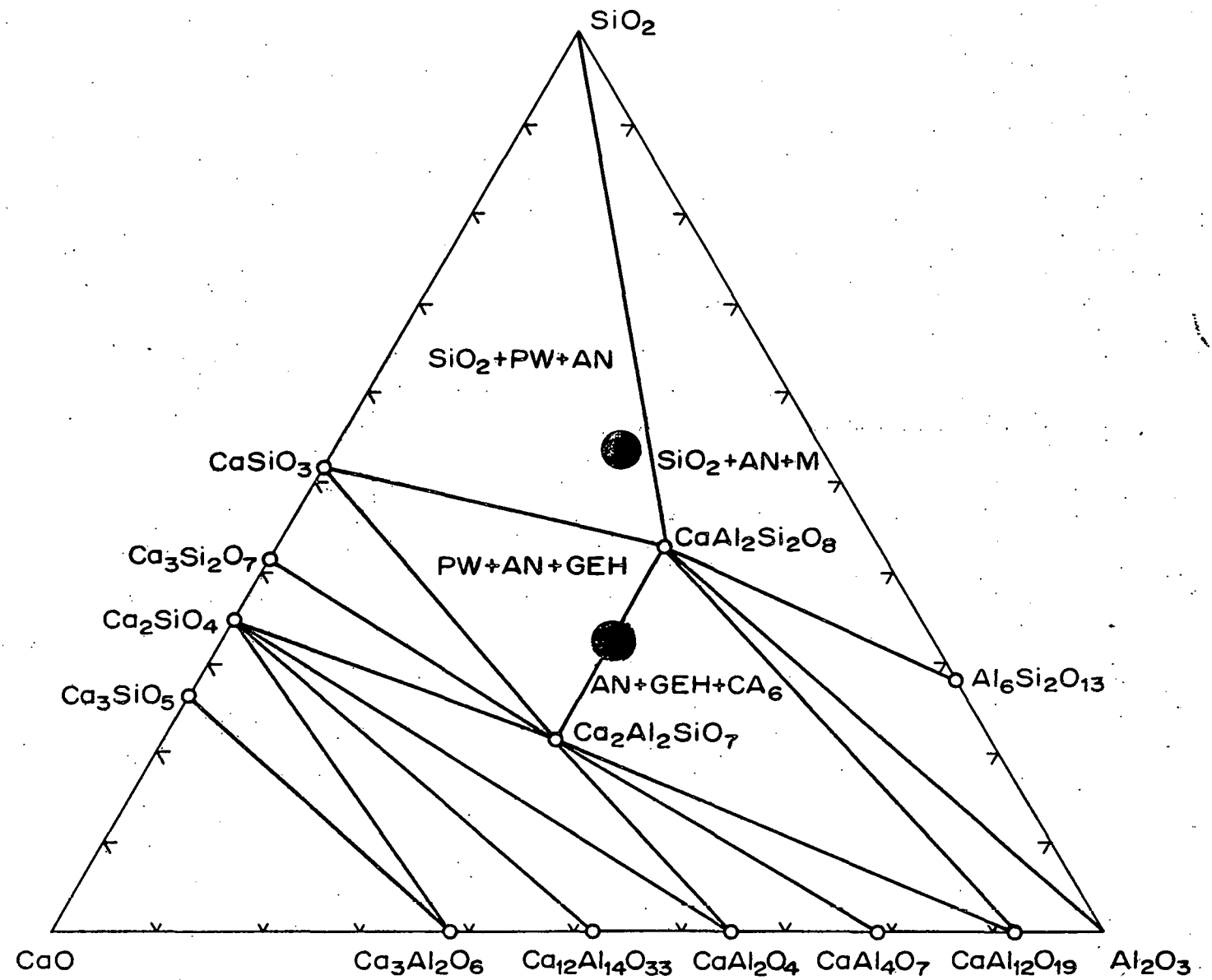
SiO2
SiO2+PW+AN
SiO2+AN+M
CaSiO3
CaAl2Si2O8
Ca3Si2O7
PW+AN+GEH
Ca2SiO4
AN+GEH+CA6
Al6Si2O13
Ca3SiO5
Ca2Al2SiO7
CaO
Ca3Al2O6
Ca12Al14O33
CaAl2O4
CaAl4O7
CaAl12O19
Al2O3

Fig. 7

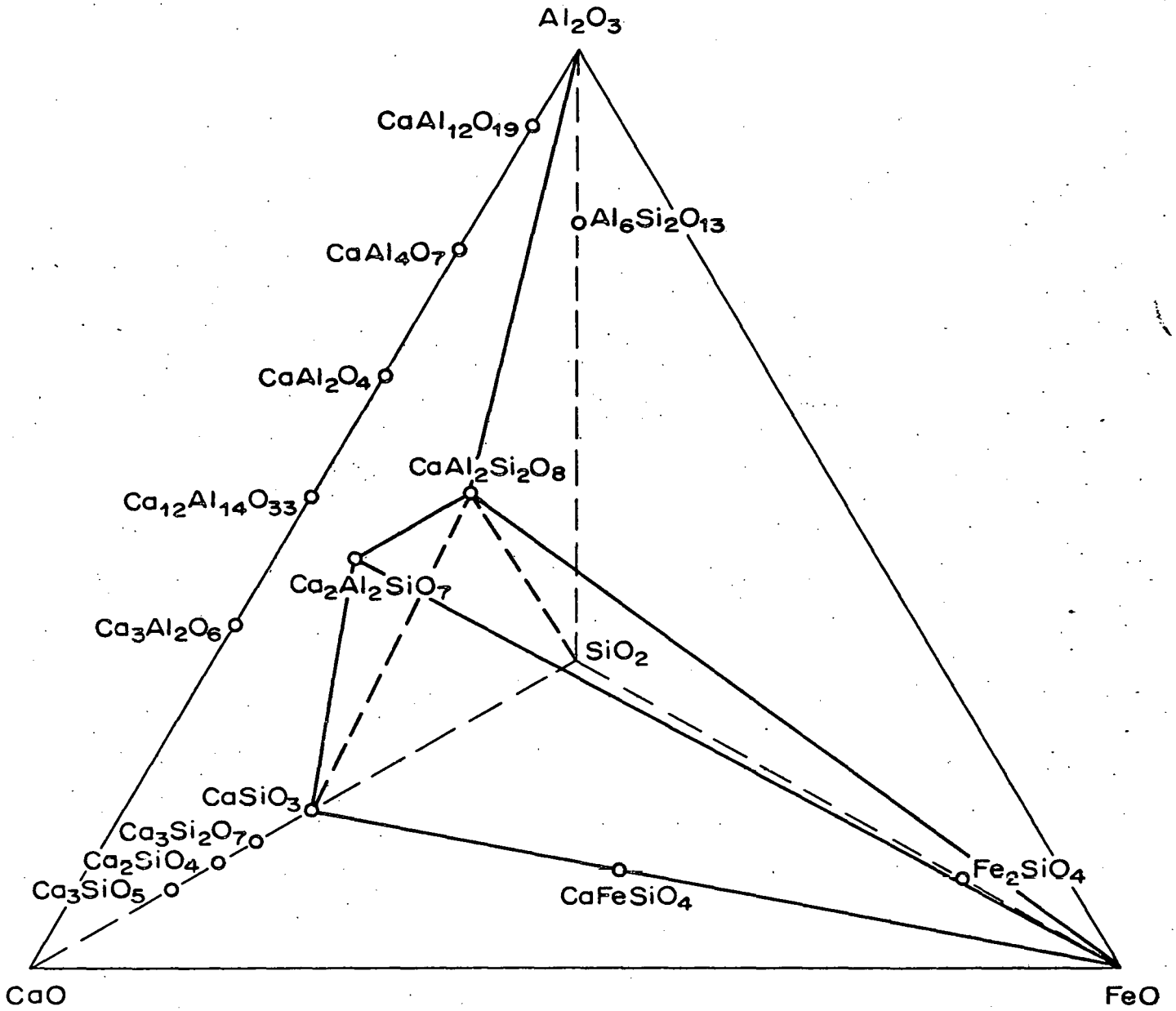
Al_2O_3
$CaAl_{12}O_{19}$
$Al_6Si_2O_{13}$
$CaAl_4O_7$
$CaAl_2O_4$
$CaAl_2Si_2O_8$
$Ca_{12}Al_{14}O_{33}$
$Ca_2Al_2SiO_7$
$Ca_3Al_2O_6$
SiO_2
$CaSiO_3$
$Ca_3Si_2O_7$
Ca_2SiO_4
Ca_3SiO_5
$CaFeSiO_4$
Fe_2SiO_4
CaO
FeO

Fig. 8

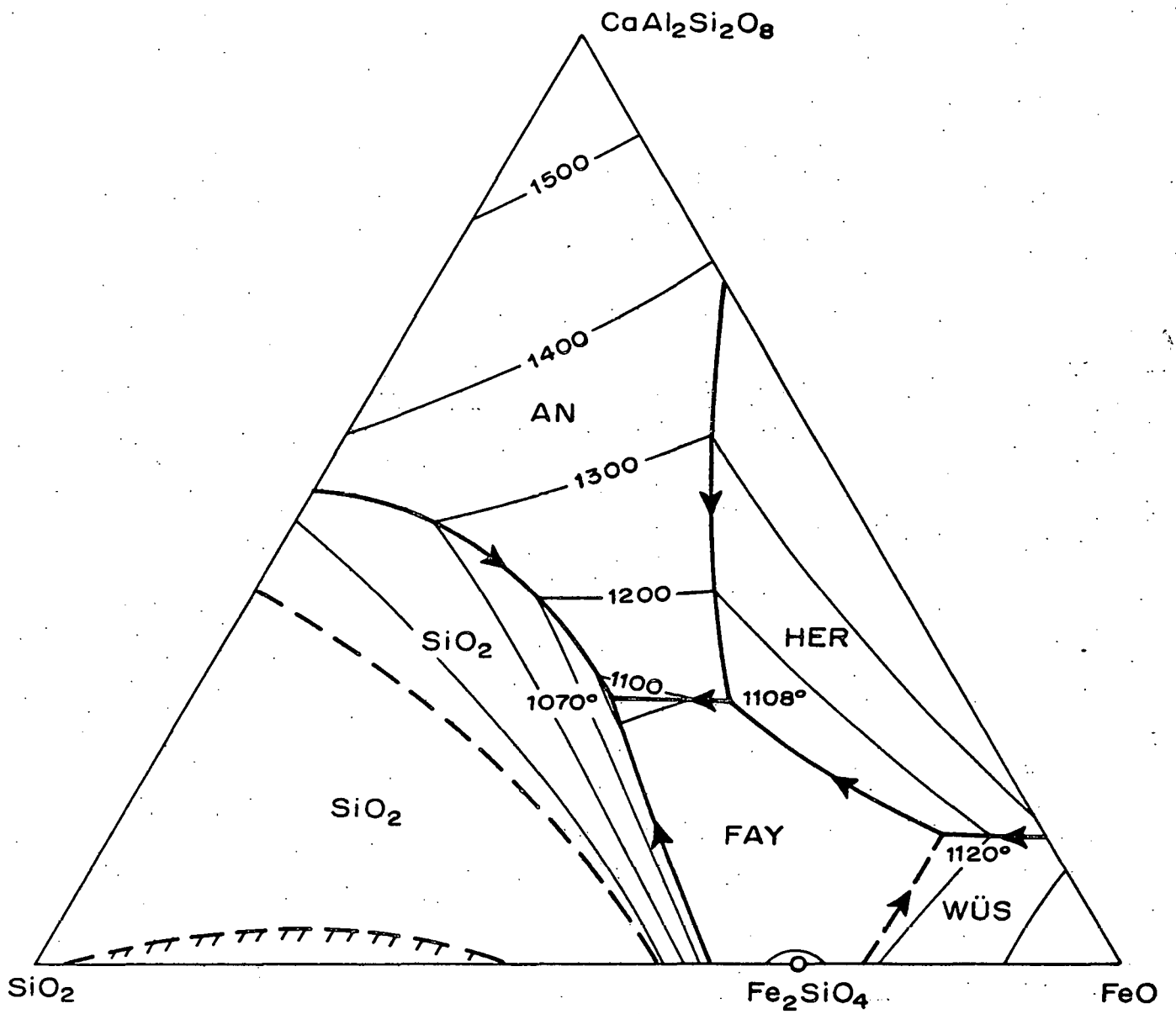
$CaAl_2Si_2O_8$
1500
1400
AN
1300
1200
SiO_2
HER
1100
1070°
1108°
SiO_2
FAY
1120°
WÜS
SiO_2
Fe_2SiO_4
FeO

Fig. 9

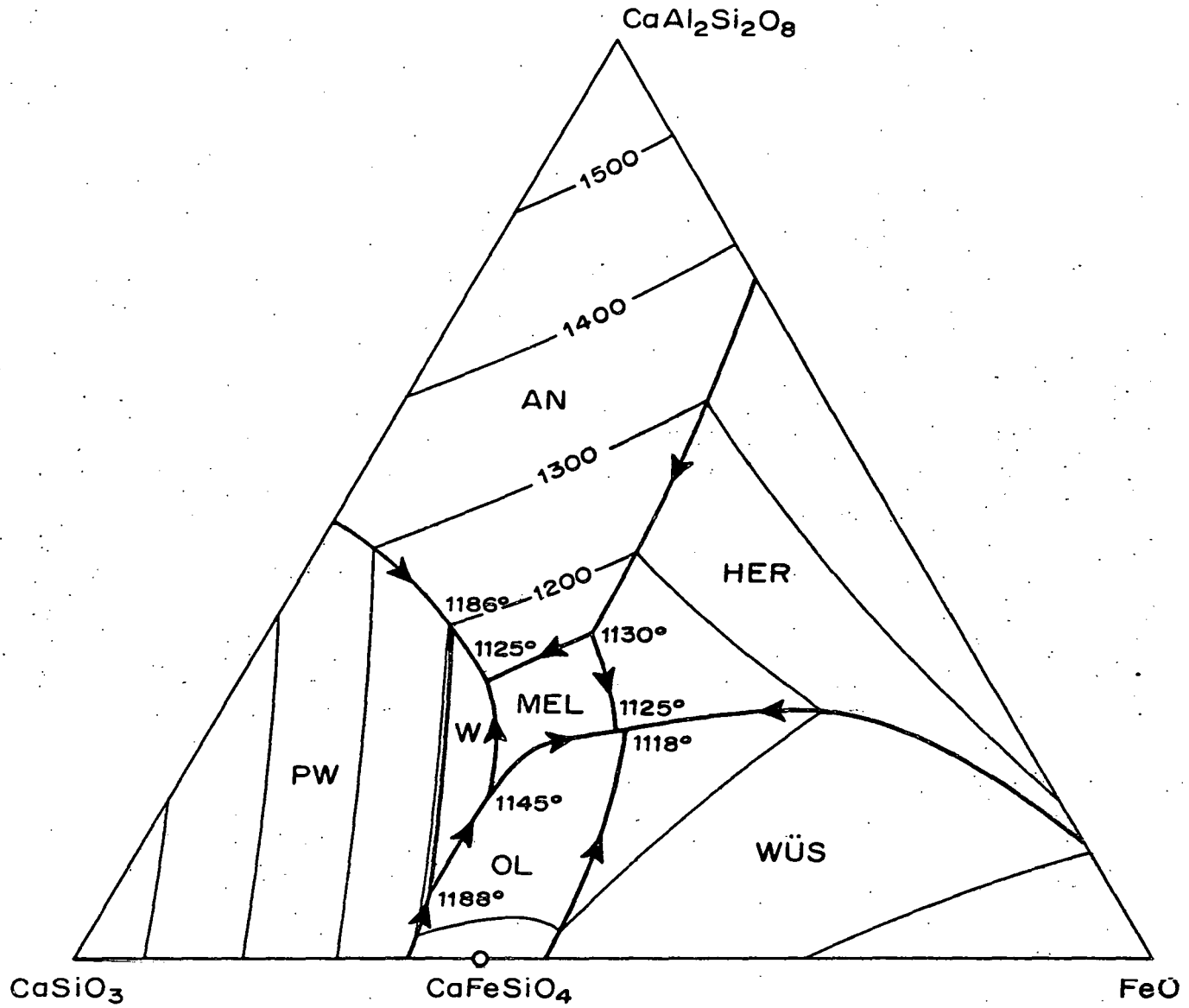
$CaAl_2Si_2O_8$
1500
1400
AN
1300
1200
HER
1186°
1125°
1130°
MEL
1125°
W
1118°
PW
1145°
OL
WÜS
1188°
$CaSiO_3$
$CaFeSiO_4$
FeO

Fig. 10

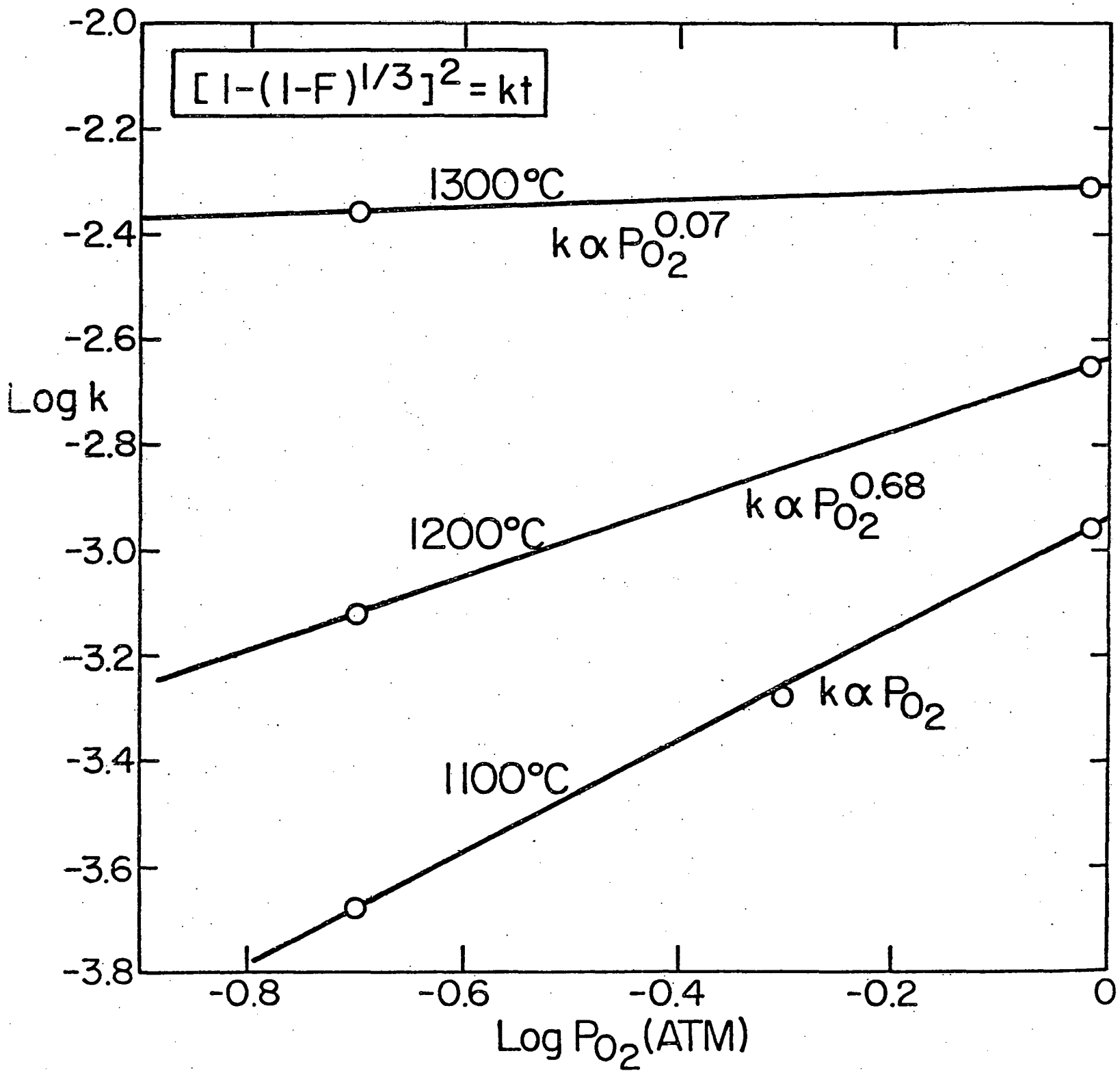
[1-(1-F)^1/3]^2 = kt
1300°C
k α P_O2^0.07
1200°C
k α P_O2^0.68
1100°C
k α P_O2
Log k
Log P_O2 (ATM)
-2.0
-2.2
-2.4
-2.6
-2.8
-3.0
-3.2
-3.4
-3.6
-3.8
-0.8
-0.6
-0.4
-0.2
0

Fig. 11

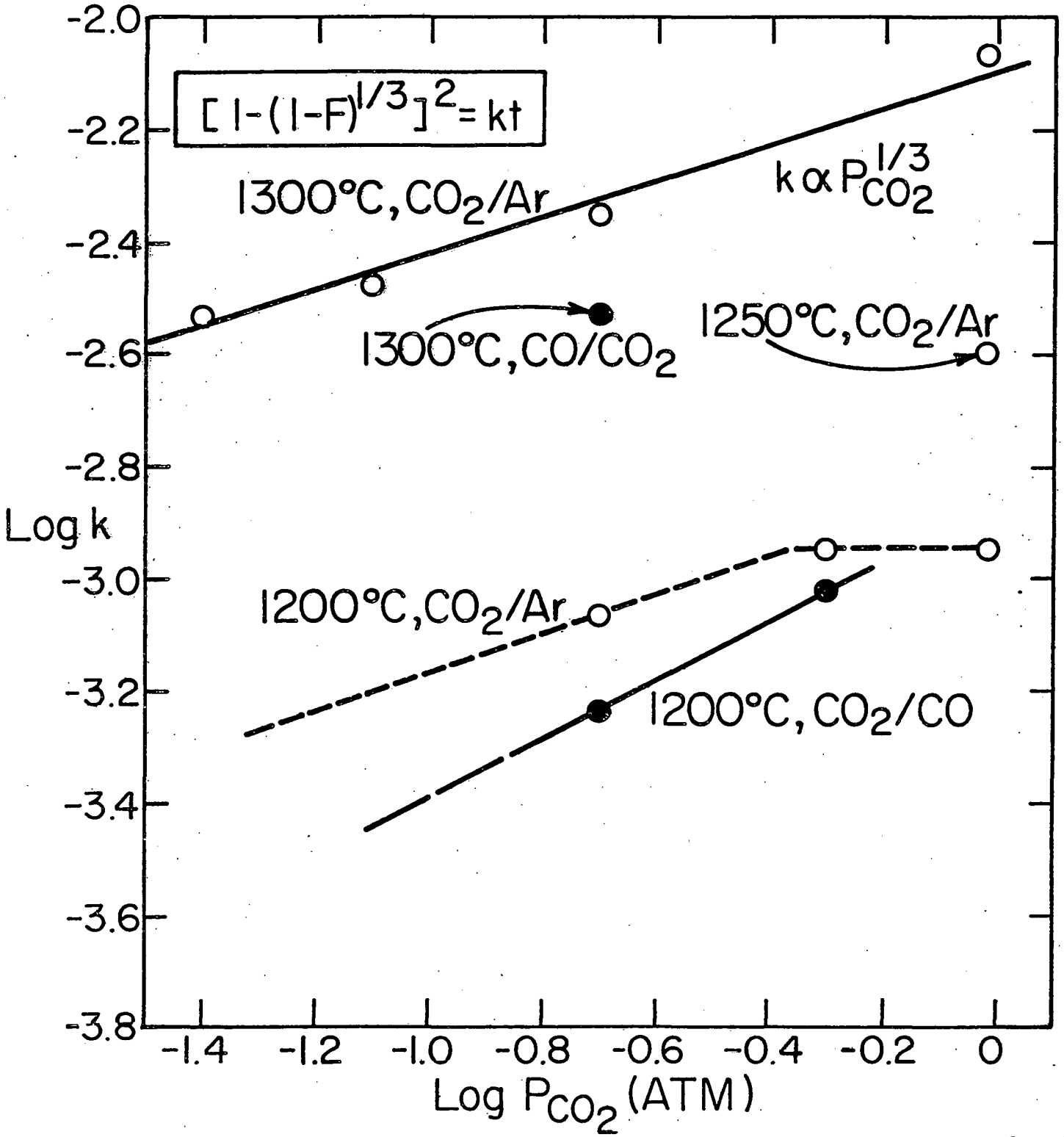
[1-(1-F)^1/3]^2 = kt
1300°C, CO2/Ar
k α P_CO2^1/3
1300°C, CO/CO2
1250°C, CO2/Ar
1200°C, CO2/Ar
1200°C, CO2/CO
Log k
Log P_CO2 (ATM)
-2.0
-2.2
-2.4
-2.6
-2.8
-3.0
-3.2
-3.4
-3.6
-3.8
-1.4
-1.2
-1.0
-0.8
-0.6
-0.4
-0.2
0

Fig. 12

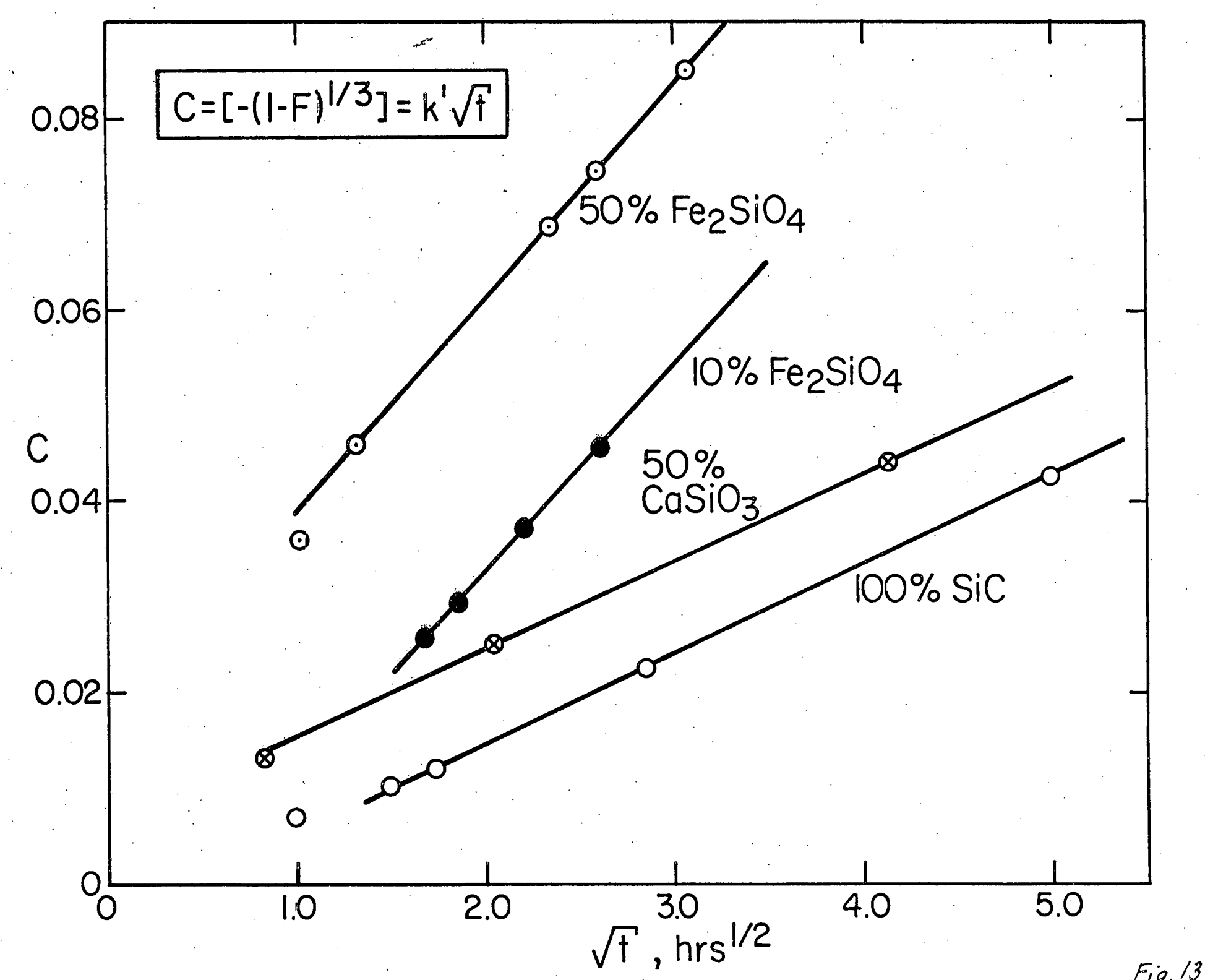
$C=[-(1-F)^{1/3}]=k'\sqrt{t}$
50% Fe_2SiO_4
10% Fe_2SiO_4
50% $CaSiO_3$
100% SiC
C
$\sqrt{t}$, $hrs^{1/2}$
0
0.02
0.04
0.06
0.08
1.0
2.0
3.0
4.0
5.0

Fig. 13

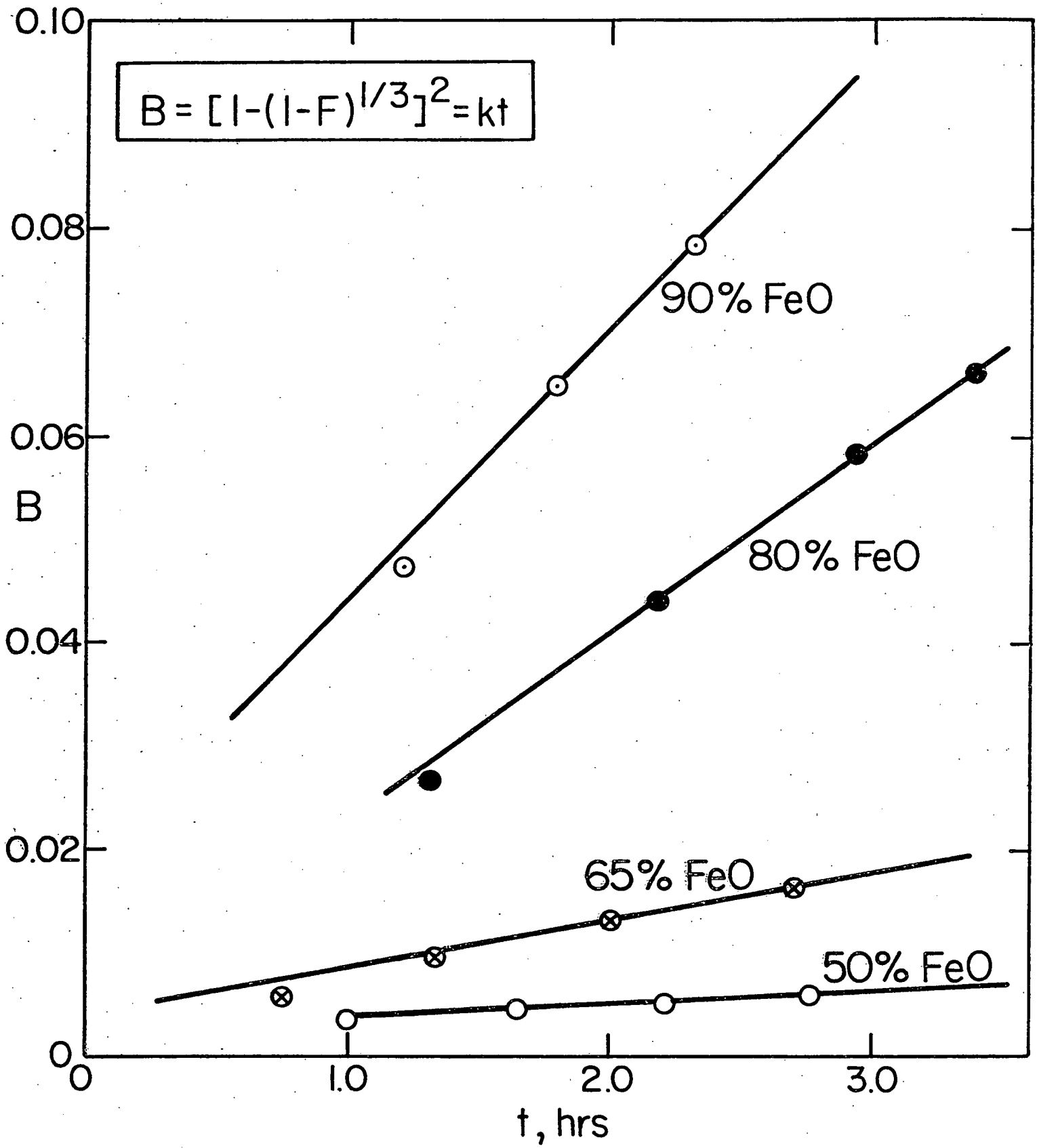
B = [1-(1-F)^1/3]^2 = kt
0.10
0.08
0.06
0.04
0.02
0
B
0
1.0
2.0
3.0
t, hrs
90% FeO
80% FeO
65% FeO
50% FeO

Fig. 14

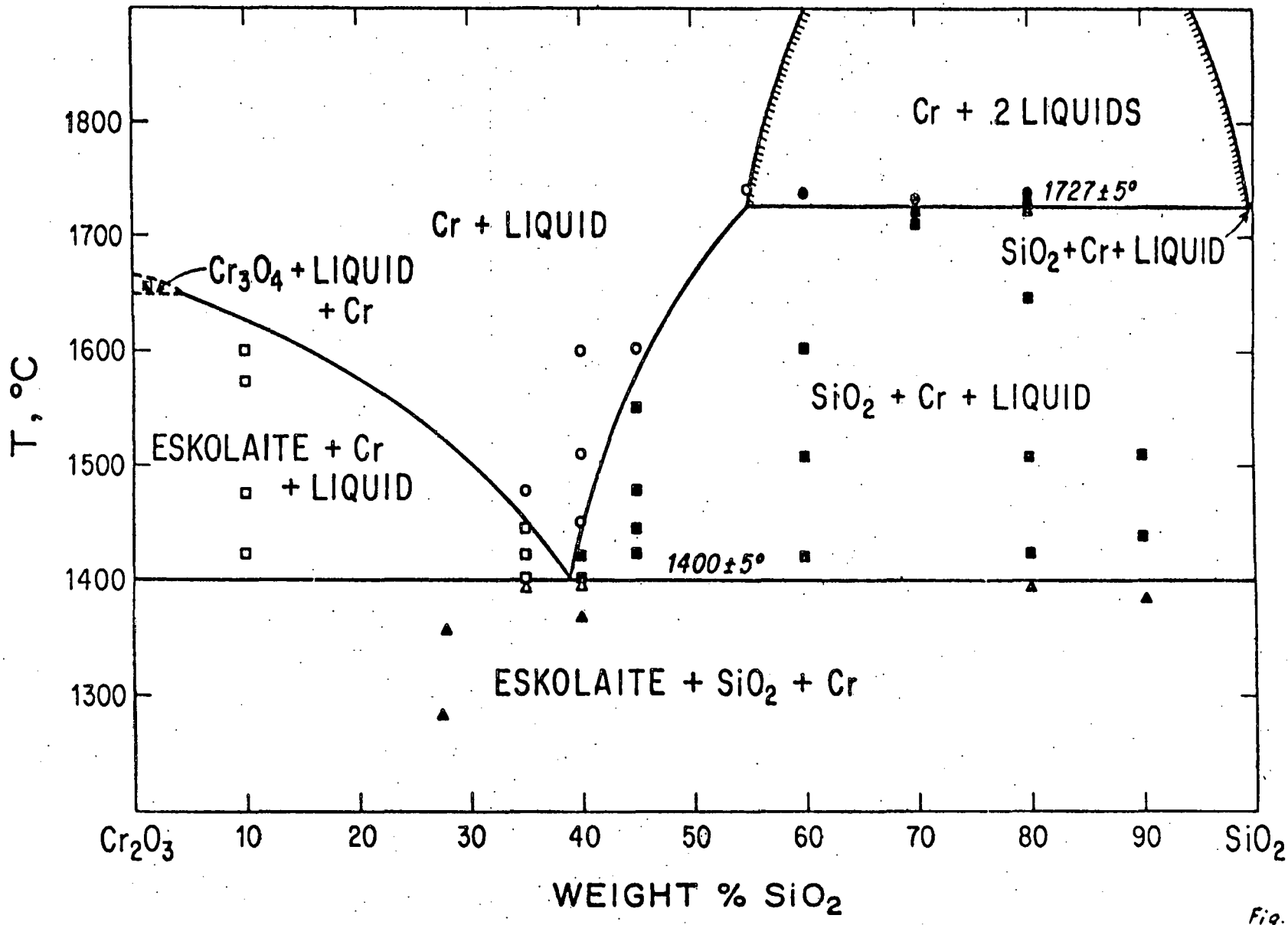
1800
1700
1600
1500
1400
1300
T, °C
Cr + 2 LIQUIDS
1727±5°
Cr + LIQUID
SiO_2+Cr+ LIQUID
Cr_3O_4 + LIQUID
+ Cr
SiO_2 + Cr + LIQUID
ESKOLAITE + Cr
+ LIQUID
1400±5°
ESKOLAITE + SiO_2 + Cr
Cr_2O_3
10
20
30
40
50
60
70
80
90
SiO_2
WEIGHT % SiO_2

Fig. 15

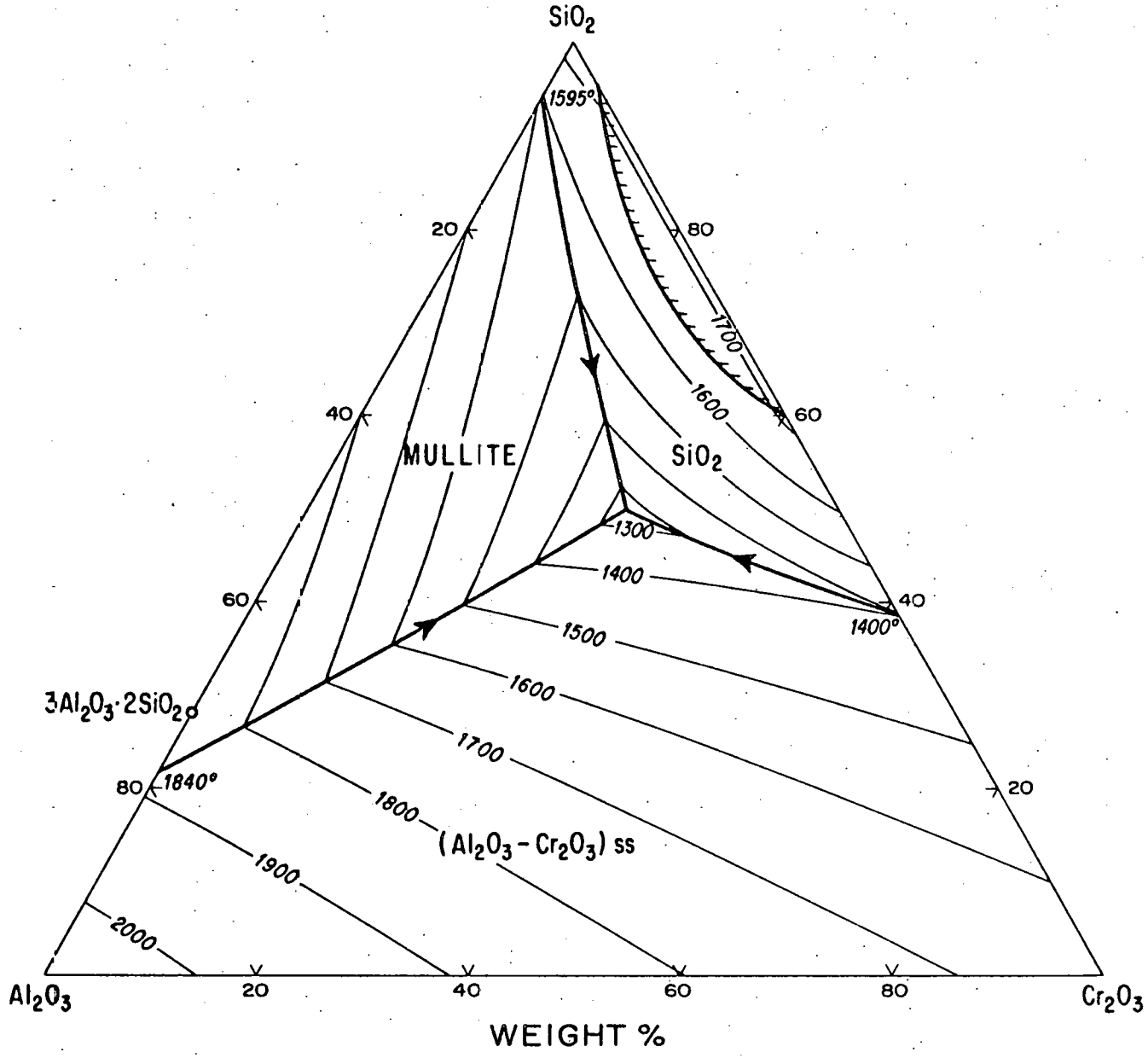
SiO2
1595°
20
80
1700
1600
40
60
MULLITE
SiO2
1300
1400
60
40
1400°
1500
3Al2O3·2SiO2
1600
1700
80
1840°
1800
(Al2O3 - Cr2O3) ss
20
1900
2000
Al2O3
20
40
60
80
Cr2O3
WEIGHT %

Fig. 16

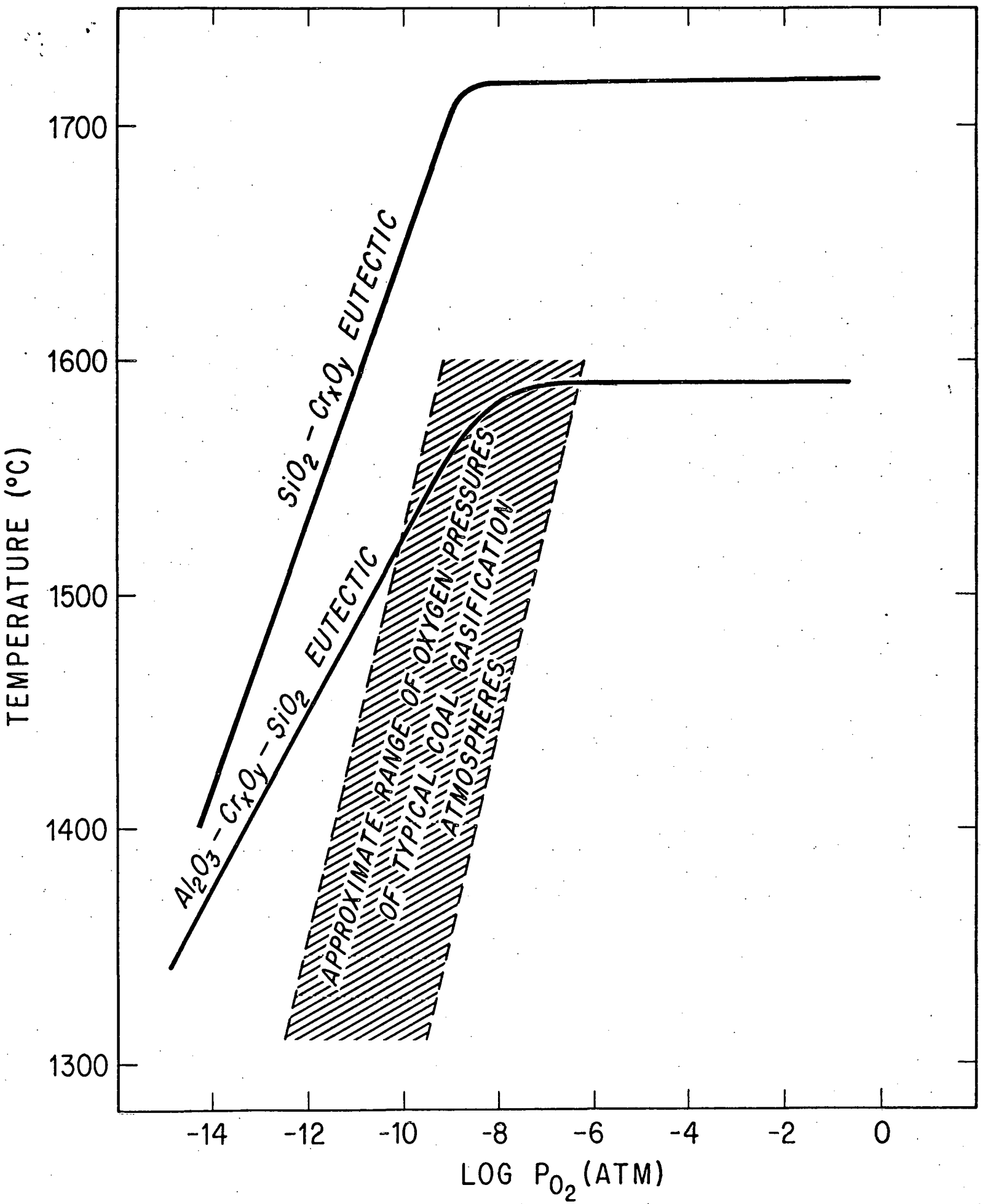
1700
1600
1500
1400
1300
TEMPERATURE (°C)
-14
-12
-10
-8
-6
-4
-2
0
LOG P_{O_2} (ATM)
$SiO_2 - Cr_xO_y$ EUTECTIC
$Al_2O_3 - Cr_xO_y - SiO_2$ EUTECTIC
APPROXIMATE RANGE OF OXYGEN PRESSURES OF TYPICAL COAL GASIFICATION ATMOSPHERES

Fig. 17

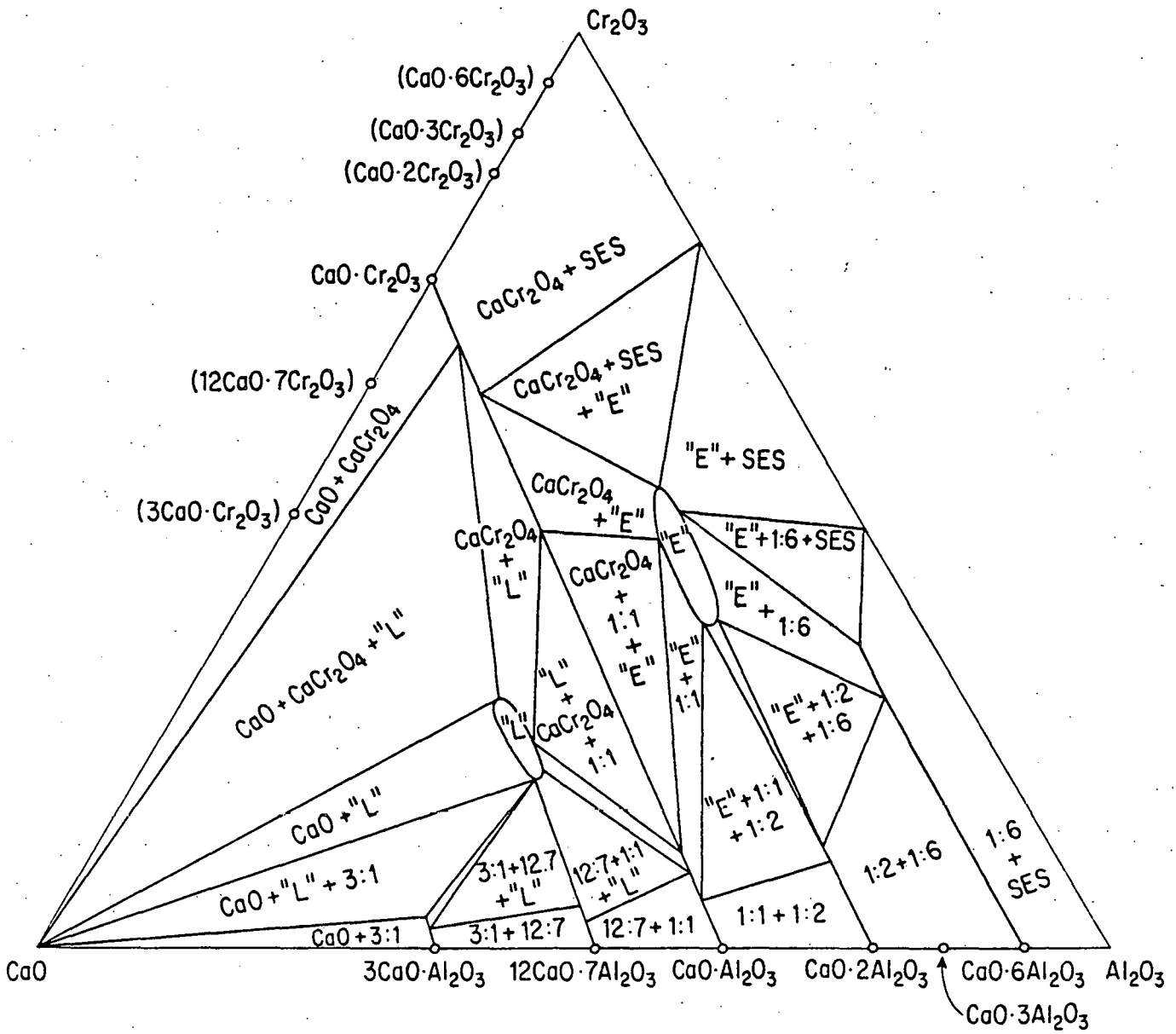
Cr_2O_3
$(CaO \cdot 6Cr_2O_3)$
$(CaO \cdot 3Cr_2O_3)$
$(CaO \cdot 2Cr_2O_3)$
$CaO \cdot Cr_2O_3$
$(12CaO \cdot 7Cr_2O_3)$
$(3CaO \cdot Cr_2O_3)$
$CaCr_2O_4$ + SES
$CaCr_2O_4$ + SES + "E"
"E" + SES
$CaCr_2O_4$ + "E"
"E"
"E" + 1:6 + SES
$CaCr_2O_4$ + "L"
$CaCr_2O_4$ + 1:1 + "E"
"E" + 1:6
"E" + 1:1
"E" + 1:2 + 1:6
"L" + $CaCr_2O_4$ + 1:1
"L"
$CaO + CaCr_2O_4$
$CaO + CaCr_2O_4 + "L"$
$CaO + "L"$
$CaO + "L" + 3:1$
$CaO + 3:1$
3:1 + 12:7 + "L"
12:7 + 1:1 + "L"
3:1 + 12:7
12:7 + 1:1
"E" + 1:1 + 1:2
1:1 + 1:2
1:2 + 1:6
1:6 + SES
CaO
$3CaO \cdot Al_2O_3$
$12CaO \cdot 7Al_2O_3$
$CaO \cdot Al_2O_3$
$CaO \cdot 2Al_2O_3$
$CaO \cdot 6Al_2O_3$
Al_2O_3
$CaO \cdot 3Al_2O_3$

Fig. 18

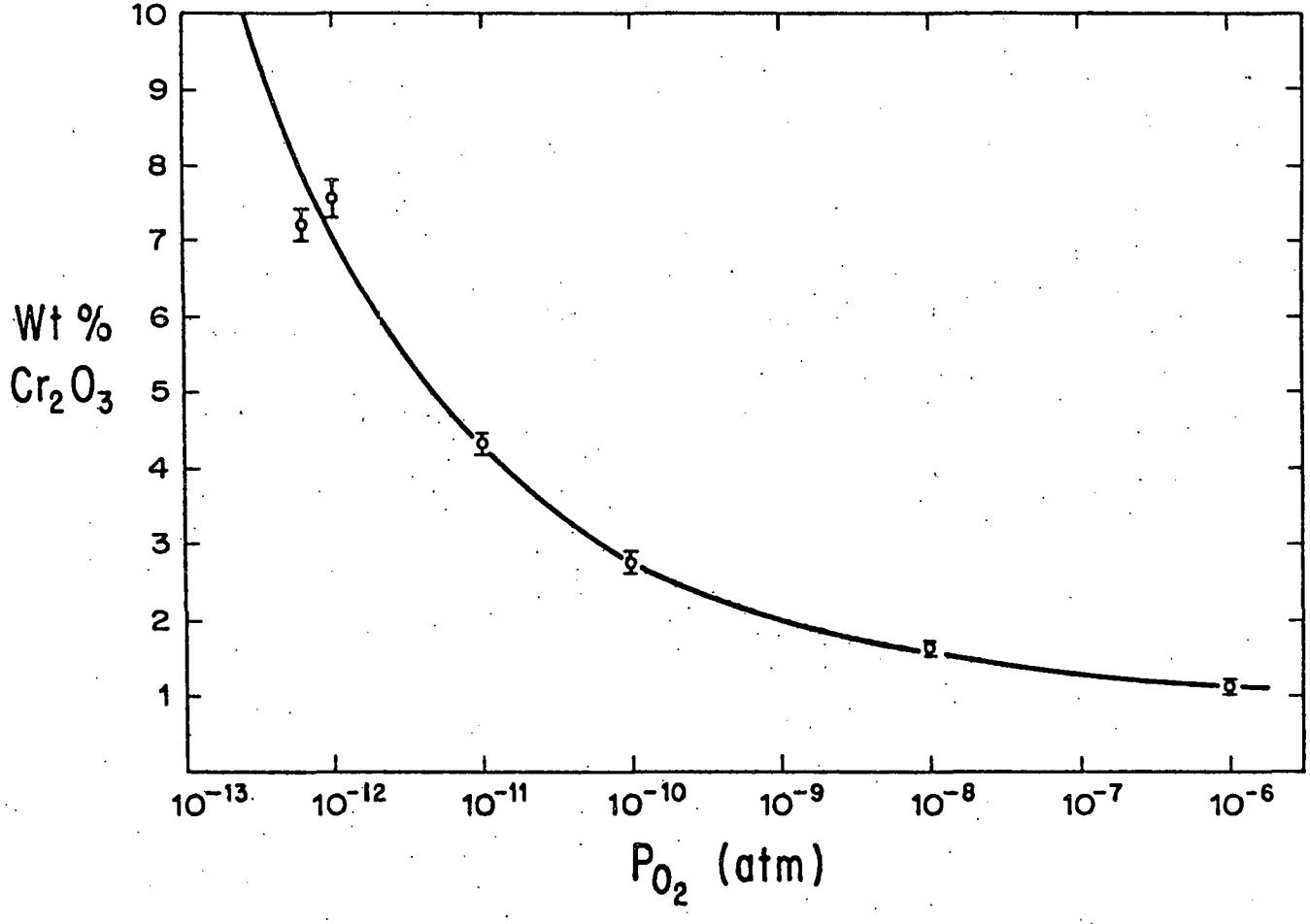
10
9
8
7
6
5
4
3
2
1
Wt %
Cr_2O_3
10^{-13}
10^{-12}
10^{-11}
10^{-10}
10^{-9}
10^{-8}
10^{-7}
10^{-6}
P_{O_2} (atm)

Fig. 19

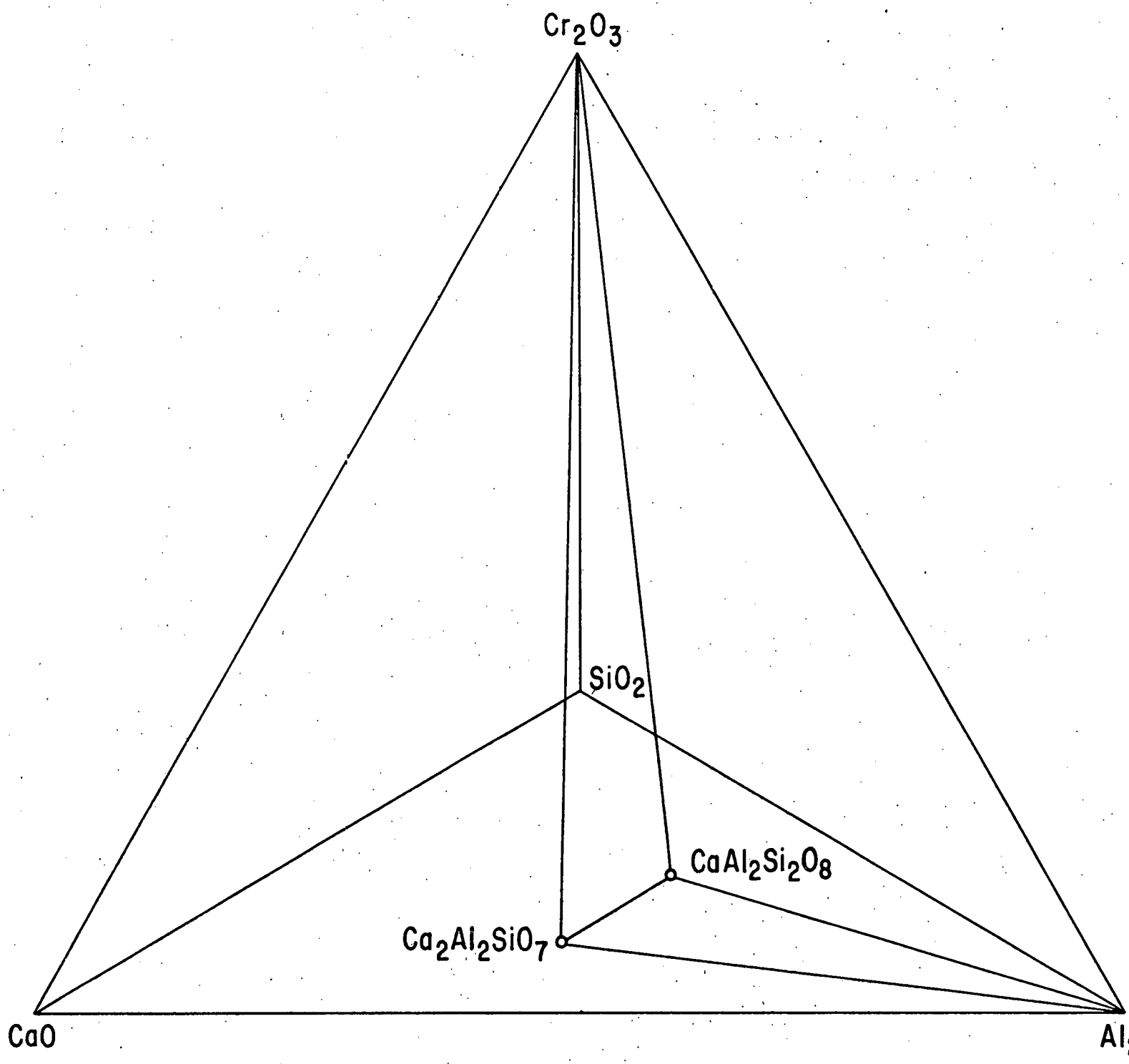

Fig. 20

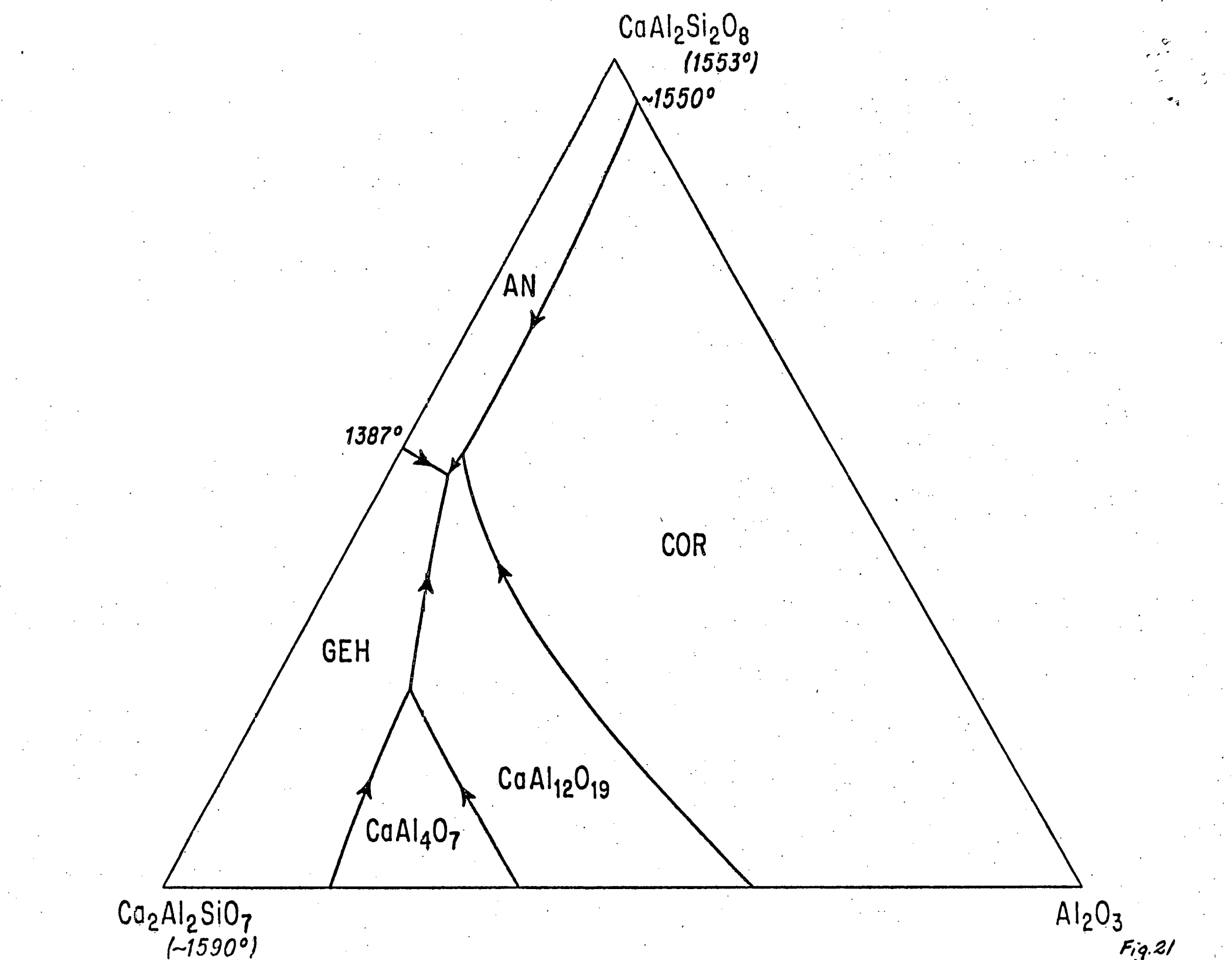
$CaAl_2Si_2O_8$
(1553°)
~1550°
AN
1387°
COR
GEH
$CaAl_{12}O_{19}$
$CaAl_4O_7$
$Ca_2Al_2SiO_7$
(~1590°)
Al_2O_3

Fig. 21

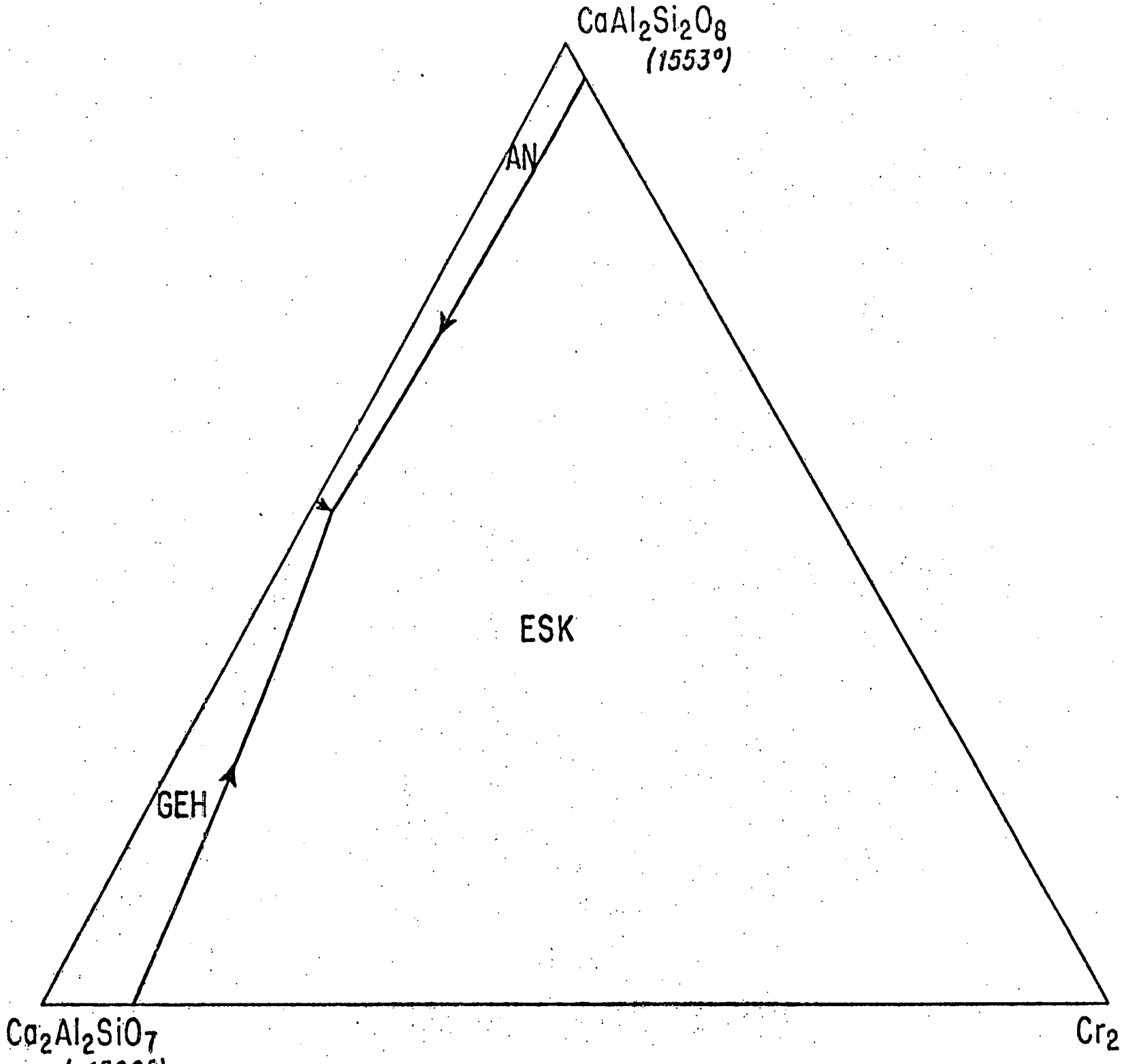

Fig. 22

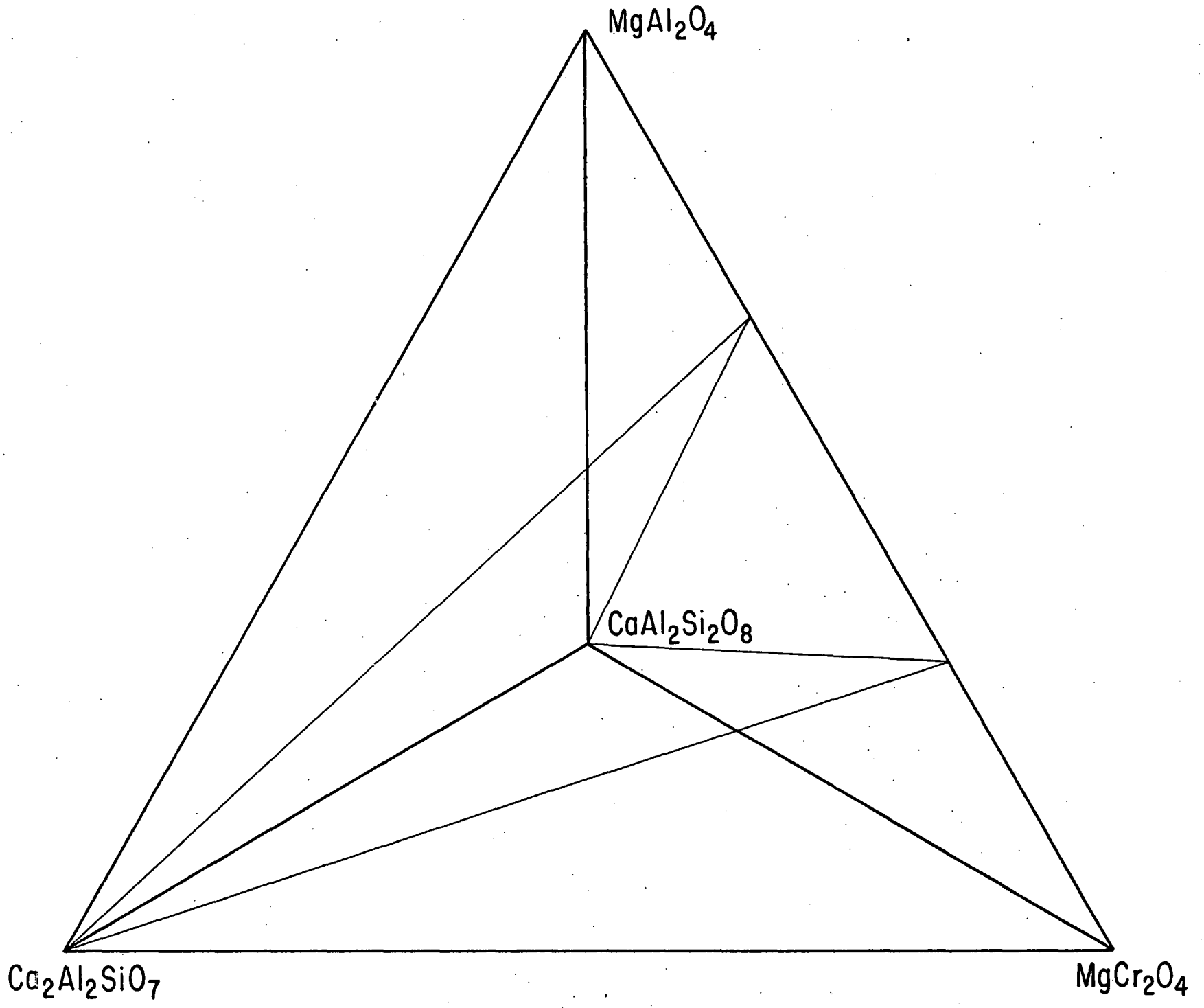

Fig. 23

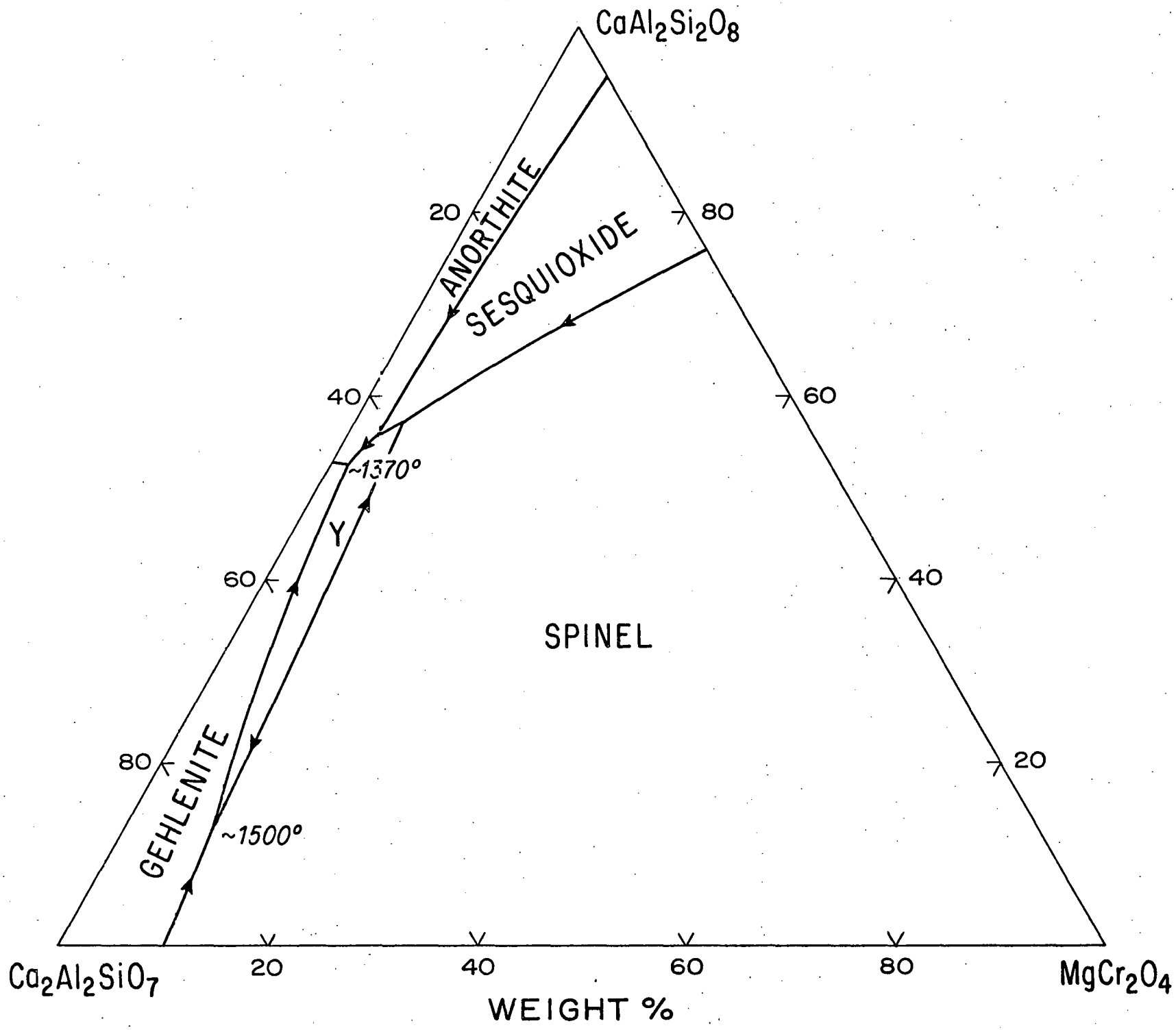
$CaAl_2Si_2O_8$
20
80
ANORTHITE
SESQUIOXIDE
40
60
~1370°
Y
60
40
SPINEL
80
20
GEHLENITE
~1500°
$Ca_2Al_2SiO_7$
20
40
60
80
$MgCr_2O_4$
WEIGHT %

Fig. 24

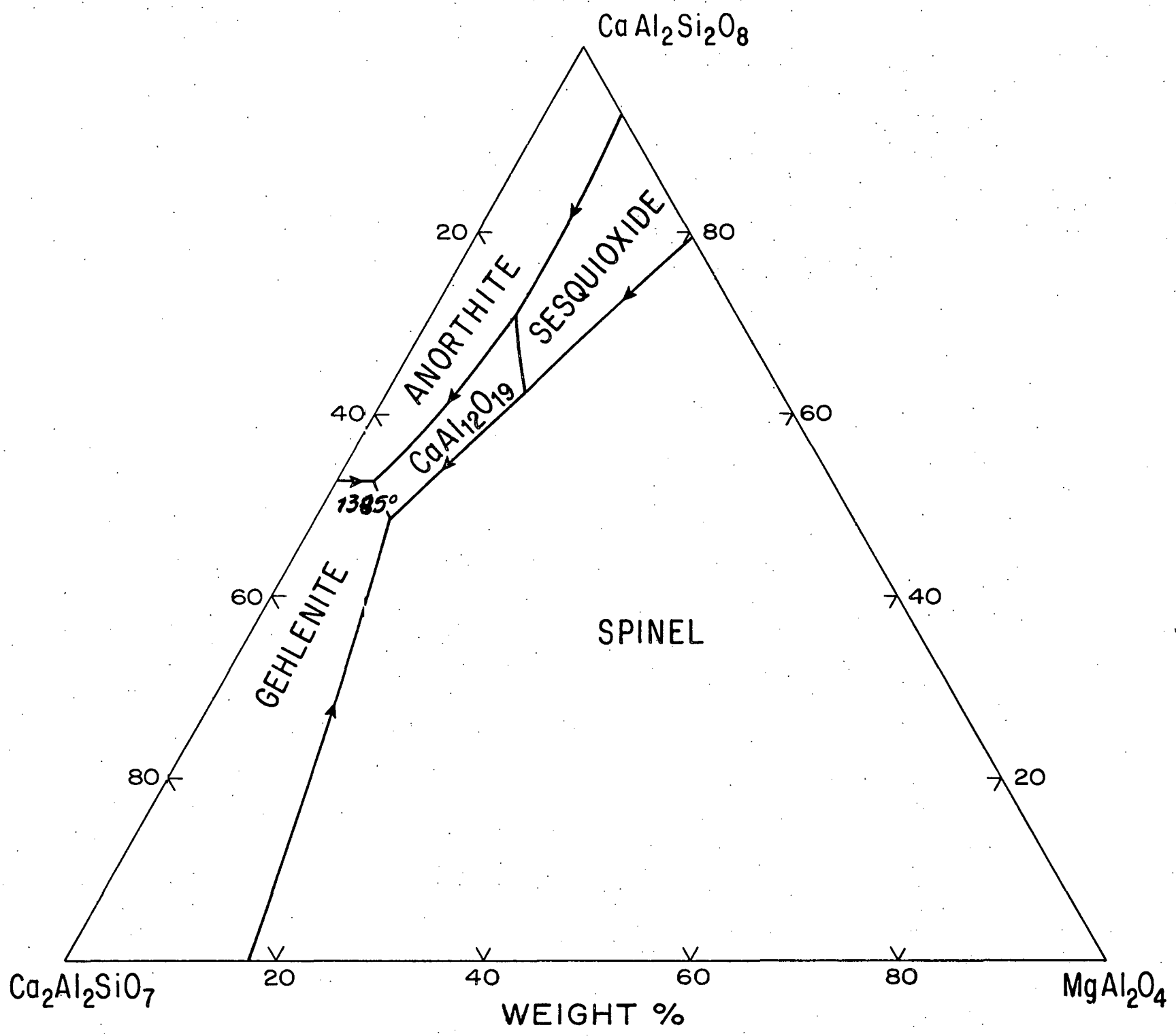
$CaAl_2Si_2O_8$
ANORTHITE
SESQUIOXIDE
$CaAl_{12}O_{19}$
1385°
GEHLENITE
SPINEL
20
40
60
80
$Ca_2Al_2SiO_7$
$MgAl_2O_4$
WEIGHT %

Fig. 25